7-1-2011

Synthesis and characterization of tethered poly(n-isopropylacrylamide) for quantitative cell adhesion studies

Phanindhar Shivapooja

Phanindhar Shivapooja
Candidate

Chemical and Nuclear Engineering
Department

This thesis is approved, and it is acceptable in quality and form for publication:

Approved by the Thesis Committee:

, Chairperson

SYNTHESIS AND CHARACTERIZATION OF TETHERED POLY(N-ISOPROPYLACRYLAMIDE) FOR QUANTITATIVE CELL ADHESION STUDIES

BY

PHANINDHAR SHIVAPOOJA

B.S., CHEMICAL ENGINEERING, 2008

THESIS

Submitted in Partial Fulfillment of the
Requirements for the Degree of

Master of Science
Chemical Engineering

The University of New Mexico
Albuquerque, New Mexico

May 2011

Dedication

This thesis is dedicated to my parents

for their love, endless support

and encouragement

Acknowledgments

Thanks to my advisor Professor Gabriel P. Lopez who always believed in me. Professor Lopez groomed me with adequate support and directions at every step of my graduate research and academic career. The two years of research experience by working in Lopez lab gave me the confidence to do independent research and thinking. Thanks to the other members of my thesis committee: Professor Heather Canavan and Professor David Whitten.

Thanks to all my friends at University of New Mexico, especially Linnea K. Ista who provided me with good guidance and support throughout my graduate research career at the Center for Biomedical Engineering.

It has been a great experience to work with all my colleagues and CBME faculty advisors, especially Professor Canavan for her guidance in my research work. I also take this opportunity to thank my group members, Dr. Sergio Mendez, Dr. Brett Andrzejewski, Dr. Menake Piyasena, Dr. Arjun Thapa, Kevin Cushing, Kyle Staggs and many other CBME students for their helpful discussions and support.

SYNTHESIS AND CHARACTERIZATION OF TETHERED POLY(N-ISOPROPYLACRYLAMIDE) FOR QUANTITATIVE CELL ADHESION STUDIES

BY

PHANINDHAR SHIVAPOOJA

ABSTRACT OF THESIS

Submitted in Partial Fulfillment of the
Requirements for the Degree of

Master of Science
Chemical Engineering

The University of New Mexico
Albuquerque, New Mexico

May 2011

SYNTHESIS AND CHARACTERIZATION OF TETHERED POLY(*N*-ISOPROPYLACRYLAMIDE) FOR QUANTITATIVE CELL ADHESION STUDIES

by

PHANINDHAR SHIVAPOOJA

B.S., Chemical Engineering, Osmania University, 2008

M.S., Chemical Engineering, University of New Mexico, 2011

Abstract

Environmentally responsive (or "smart") polymers represent a new approach for controlling biofouling release. Poly(*N*-isopropylacrylamide) (PNIPAAm) is a thermo responsive polymer that can potentially be used to control biofouling, as it exhibits a change in its relative hydrophobicity above and below its lower critical solution temperature (LCST ~ 32°C). This thesis reports on grafted PNIPAAm brushes, synthesized using a relatively simple and rapid method which allows atom transfer radical polymerization (ATRP) in presence of air. In this study the structure, purity and thermally responsive behavior of grafted brushes have been characterized using X-ray photoelectron spectroscopy, time-of-flight secondary ion mass spectroscopy, Fourier

transform infra-red spectroscopy, ellipsometry and contact angle measurements. Together all these studies proved that uniform, controlled and high molecular weight PNIPAAm brushes can be produced using ARGET ATRP.

A quantitative study of detachment of marine bacteria from these surfaces, both above and below the LCST using a spinning disc apparatus is also reported. This device applies a linear range of reproducible shear forces to cells attached at the interface of a single sample. In this work, a model marine bacterium, *Cobetia marina* which adheres more readily to hydrophobic surfaces was attached to PNIPAAm grafted surfaces at 37°C and subjected to varied detachment forces in artificial sea water. We found that the number of adherent cells decreased non-linearly with applied force and the cell detachment at the interface required lesser shear force at lower temperatures evaluated. The ability to directly correlate a measurable force to bacterial attachment and release represents a step forward in understanding of interactions between PNIPAAm and bacterial cells. Our work demonstrates the potential of stimuli responsive polymers as possible fouling-release agents, and suggests that grafted PNIPAAm (or similar polymers) may be useful as regenerable fouling-release surfaces.

Table of Contents

List of Figures

Chapter 1

Introduction

1.1 Biofouling

1.1.1 General

Biofouling can be defined as the unwanted deposition and growth of organisms that adhered to a surface, often in a biofilm [1-4]. Biofouling is a worldwide problem, encountered in an extremely wide range of situations, and is generally problematic in various human endeavors including paper and pulp industries, natural gas and petroleum industries, food processing and packaging, cooling towers, implanted biomaterials, membrane technologies, underwater constructions and sensors, heat exchangers, and water desalination systems [5-7]. For example, in cooling water circuits, the presence of biofilms can alter surface roughness, which in turn can increase fluid frictional resistance resulting in decreased flow rates [8]. They also effect the heat transfer in heat exchangers, increase pressure drop, [9, 10] enhance corrosion [11] and act as a source of pathogenic contamination [12]. Biofilms can also associated with medical devices and medical implants, formed by the plethora of environmental bacteria that opportunistically infect a host which is compromised by injury or medical intervention [13-15]. Thus, biofouling is

a serious problem affecting a multitude of industrial processes and limiting the performances of devices in numerous applications.

1.1.2 Marine biofouling

One of the most common biofouling sites is on the hulls of ships, where barnacles and algae are often found. In sea water, the underlying phenomenon of biofouling can be divided into: (1) microfouling: biofilms formed by bacteria, fungi and diatoms (2) macrofouling: attachment of macroalgae and invertebrates, particularly barnacles, mussels, polychaete worms, and bryozoans. Together, these organisms form a fouling community [2]. In order to analyze and control the various problems associated with biofouling, it is good to briefly understand the basics of biofilms formation and development [5].

Upon submersion in a non-sterile aqueous liquid, most surfaces become rapidly colonized by bacteria and other micro-organisms within hours. Initially, suspended or motile bacteria are attracted towards these surfaces and are held to the substratum by weak electrostatic forces, hydrogen bonds and van der Waals interactions [16, 17]. After adhesion, the cells produce a layer of extracellular polymeric substances (EPS), highly hydrated biopolymers of microbial origin such as polysaccharides, proteins and nucleic acids. In this matrix they organize their life, develop complex interactions, including the resistance to biocides [1, 6]. The structure of the resulting biofilm is highly heterogeneous, dynamic and provides ecological advantages for the biofilm mode of life.

Attachment of macroalgae is more complicated and involves a number of sequential events [1, 2]. For the majority of algae, initial contact with a substratum is achieved by specialized reproductive propagules which can be either motile or non-motile. Following the initial attachment process, all spores secrete an adhesive material which permanently secures the spores to the substratum. The attached spores germinate to produce a primary rhizoid system which is responsible for the attachment of the seaweeds. The attachment mechanism and adhesives of macrofouling invertebrates are even more complex than those of bacteria and algae due to the metamorphic life cycle [18]. Water flow, mechanical damage and various other environmental factors can influence biofilm formation and community development [19]. As such, fouling can be considered highly dynamic process [20].

The practical consequence of colonization followed by biofilm formation and development by these complex surface attached communities is biofouling. The most obvious problem of biofouling on a ship is the eventual corrosion of the hull, leading to the ship's deterioration. It is a worldwide problem in marine systems, costing the US Navy alone an estimated $1 billion per annum [21]. On hulls, biofouling also results in an increase in roughness, which in turn leads to an increase in hydrodynamic drag as the vessels moves through water [22]. High frictional resistance due to roughness leads to an increase in drag and weight, followed by subsequent potential speed reduction and loss of maneuverability of the ships. This in turn has economic and environmental consequences, as increased fuel consumption leads to increased output of greenhouse gases. The US Naval Sea Systems Command estimates that biofouling on ship hulls results in a speed

loss of approximately 2% and increases fuel costs by 6 to 45% depending on the size of the ship [23]. Additionally, attached organisms (e.g. mussels) are introduced into environments where they were not naturally present (invasive and non-native species) [24, 25]. Typical method of cleaning fouling from ships in dry-dock reduces the vessel's useful operation time and adds to the cost of maintenance. A large amount of toxic waste is also generated during this process [26].

Parts of ship other than the hull are also affected, such as heat exchangers, water-cooling pipes and propellers. For example, sea water also comes into contact with the interior of vessels during its use as a coolant for ships' power plants; the buildup of microbial biofouling on heat transfer equipment can lead to drastic reductions in efficiency, up to 30%, in a matter of months [27].

1.2 Approaches to control biofouling

There are three principal approaches [28] to control biofouling: (1) mechanical detachment of biofoulers, if possible; (2) killing, inactivation or removal of biofouling organisms, using antibiotics, biocides and cleaning chemicals, and (3) surface modification with the aim of turning the substrate materials into a low-fouling or non-sticking (non-adhesive) one. Many researchers are focusing on non-toxic biofouling control strategies based mainly on the third approach, i.e. on the idea of creating low-fouling or non-adhesive materials [5].

1.2.1 Conventional

Typical conventional methods include the use of wipers, scrapers, and other mechanical systems, which generally leads to mechanical failure of the equipment. As cleaning (or scraping) of biofouled surfaces is a time consuming process with limited effectiveness, antifouling coatings have been the primary strategy for combating biofouling in the marine industry.

Biocides such as tributyltin (TBT) were developed in the mid-20th century and were the active components of antifouling paints until recently [29]. Biocidal coatings based on tributyltin self-polishing copolymer paints (TBT-SPC) have been effective at reducing biofouling [25, 29, 30]. Nevertheless, TBT-based paints are highly toxic for many aquatic organisms and have been proven to contaminate the food chains and to be persistent in the environment [31]. For example, it has been shown that even extremely low concentrations of TBT caused defective shell growth in the oyster *Crassostrea gigas* [32] and imposex (development of male characteristics in female organism) in the dog-whelk *Nucella canaliculata* [33]. These kinds of detrimental effects on non-target organisms and the surrounding environment resulted in the prohibition of the use of TBT-based paints by many nations [34] (e.g., Amendment to Marketing and Use Directive (76/769/EEC)). The response to this ban has been the use of copper, zinc, and a variety of organic compounds as the active, antifouling components. However, due to the release of these ions from the coated surfaces there is evidence indicating the presence of these compounds in marinas and harbors, and there potential responsibility for the same

negative effects as TBT [35]. In addition, it has been proved that bacteria which are in contact with antifouling coatings can rapidly develop resistances to biocides, especially in estuaries [36, 37], where most of the boats and aquaculture structures are moored.

1.2.2 Emerging

Due to the concerns about environmental pollution and unintentional poisoning of marine organisms, many researchers have now focused on developing environmentally friendly coatings that are non-toxic and can exhibit antifouling or fouling-release properties.

Fouling resistant surfaces: There are natural surfaces that resist biofouling in the marine and biomedical environments. Many marine organisms such as sharks, mussels, crabs and the endothelium of mammalian heart artery have natural antifouling defenses. Based on this idea, natural fouling resistant compounds were isolated from marine plants that are not colonized by bacteria [38]. For example, Steinberg *et al.* [39] have isolated signaling molecules from an Australian seaweed exhibiting anti-colonizing activity. Many natural anti-fouling products have been investigated, but the problems with these compounds are that most of them are only scarcely available, they lose their antifouling characteristics due to age and they are difficult to apply on a consistent and constant basis on a surface [40, 41].

Surface chemistry is a significant factor in adhesion of fouling organisms to surfaces. For example, Baier *et al.* proposed the correlation between relative adhesion of fouling organisms and the energy of the surface [42]. One way of systematically studying

surface energy without altering the bulk properties of a coating material is through the use of self-assembled monolayers (SAMs). Whitesides and co-workers have tested the ability of a wide range of SAM chemistries to resist cell and protein adhesion [43]. Grunze *et al.* have proposed that the chain confirmation and packing of SAMs affect the penetration of water into SAM surface and are also important determinants of resistance to cell adhesion [44, 45]. Lopez and co-workers used SAMs to examine the effects of surface physico-chemistry on attachment of marine bacteria and other fouling organisms on SAMs [45-48]. For example, Ista *et al.* observed that the marine bacterium, *Cobetia marina*, attached more readily to hydrophobic surfaces and that attachment proceeded linearly with respect to decreasing surface energy on a series of SAMs composed of methyl terminated thiols diluted with either hydroxyl or carboxylic acid terminated thiolates [49]. It is clear that cell adhesion and subsequent biofouling are strongly influenced by surface chemistry of SAMs and thus, these surfaces can be used as a facile way to screen/develop new materials with excellent antifouling properties.

Fouling release surfaces: In recent years, there has been emphasis on developing non-toxic surfaces from which fouling can be readily removed (fouling release surfaces). Generally silicone elastomers and fluoropolymers, have been shown to be useful in controlling not only bacteria and algal fouling (microfouling) but also the accumulation of barnacles and other mollusks (macrofouling) [50]. Poly(dimethylsiloxane)-based fouling-release coatings show excellent fouling release properties due to their low surface energy, low micro-roughness, high elastic modulus and low glass transition temperature [33].

Lopez *et al.* have explored the possibility of using stimuli-responsive "smart" polymers as a new class of compounds for fouling release properties [49, 51-53]. Stimuli-responsive polymeric materials [54], which can respond to changes in temperature, pH, light, and ionic strength, have been widely utilized in developing intelligent or smart materials with great promise in drug delivery systems [3, 7, 55], microfluidic devices [15], and bioadhesion mediators [53, 56, 57]. Among these, poly(*N*-isopropylacrylamide) (PNIPAAm) is one of the well-studied biocompatible and thermally responsive polymer, which undergoes a sharp and reversible coil - globule phase transition in water at ~ 32°C, changing from a hydrophilic state below this temperature to a hydrophilic state above it [58]. The phase transition arises from the entropic gain as water molecules associated with the side-chain isopropyl moieties are released into the bulk aqueous phase as the temperature increases past a critical point [54]. The temperature at which this occurs (the lower critical solution temperature, LCST) corresponds to the region in the phase diagram at which the enthalpic contribution of water hydrogen-bonded to the polymer chains becomes less than the entropic gain of the system as a whole and thus is largely dependent on the hydrogen-bonding capabilities of the constituent monomer units [59].

The use of grafted PNIPAm homopolymers brushes as mediators of prokaryotic cell adhesion was first reported by Lopez and co-workers. LCST mediated transitions of surface grafted PNIPAm homopolymer materials resulted in reversible attachment and detachment of adsorbed marine bacteria (e.g., *Staphylococcus epidermidis*, *Halomonas marina*) and biofilms dependent on the inherent preferences of the bacterial strains for hydrophilic or hydrophobic substrates [49, 51-53].

1.3 Goals of this Work

The aim of our research work is to develop novel, environmental friendly thermo-responsive polymer coatings to control the initial bacterial attachment to the substratum and the early stages of biofilm formation, with an overall goal to provide a comprehensive approach to reduce biofouling. Our interest in PNIPAAm thermo-responsive polymer is because of its varying surface hydrophobicity in aqueous solution above and below a critical temperature and thereby, allowing reversibly attachment and release of marine microbes and other fouling organisms. The goals of the work presented in this thesis are focused towards two main aspects. Firstly, to develop new synthetic and convenient protocols for the synthesis of well defined PNIPAAm grafted surfaces using controlled radical polymerization techniques. Secondly, to understand the adhesion of marine bacteria to these thermo-responsive polymers under shear environment. The work also included various complementary analytical techniques to study the structure and dynamics of grafted surfaces. Quantitative analysis of cell adhesion to grafted polymer brushes was studied using various governing parameters.

Chapter 2

New Method of Synthesis and Characterization of PNIPAAm Grafted Surfaces Using ARGET ATRP in Presence of Air for Cell Adhesion Studies

2.1 Introduction

Stimuli responsive surfaces are capable of reversibly changing their properties in response to external stimuli. Polymer brushes have been explored as ideal candidates for the chemical design of responsive surfaces [60-62]. A stimulus-responsive polymer brush is a surface to which linear chains of polymer are end-grafted at such controlled high densities that the chains stretch away from the grafting surface while still retaining sufficient conformational freedom to allow a significant conformational response to small changes in external conditions, such as temperature, pH, or light. Simple end-grafted homopolymer brushes exhibit some intriguing responsive behaviors [60-62].

Poly(*N*-isopropylacrylamide) (PNIPAAm) is perhaps the most studied thermo-responsive polymer that has been used in a plethora of applications [63-65]. In this case, the term thermo-responsive is used to indicate that PNIPAAm in aqueous solution

exhibits a lower critical solution temperature (LCST) at ~32°C. The chemical structure of the polymer repeat unit is shown in Fig. 2.1. PNIPAAm in various forms (e.g. free, adsorbed, tethered, cross-linked gel) has been used in applications which include drug delivery [66-68], membrane porosity [69], chromatographic separations [70], controlling the adhesion of platelets [71], cells [52], and proteins [72], and to switch hydrophobicity [73]. We are interested in grafting PNIPAAm on flat surfaces to switch surface properties by varying the temperature through the LCST to control attachment and release of marine micro-organisms and biofilms in a reversible manner [49, 52].

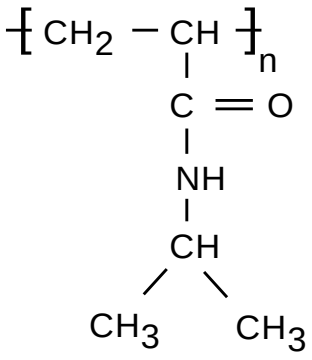

Fig. 2.1: Structure of poly(*N*-isopropylacrylamide).

To create surface grafted polymer brush, we used a "grafting from" approach, in which the polymer chain is initiated from a surface through immobilization of a monolayer of surface-initiator followed by *in situ* polymerization. By using such surface-initiated polymerization techniques, it is possible to synthesize polymer brushes with tunable grafting density, thickness, and polydispersities from a large variety of monomers [74-76].

Chapter 2

Atom transfer radical polymerization (ATRP) is now a frequently used surface-initiated polymerization process for grafting of well-defined polymers on substrates under robust conditions [77]. ATRP which is an extension of atom transfer radical addition [78], is a "controlled/living" radical polymerization method developed in 1995 by the groups of Matyjaszewski [79] and Sawamoto [80]. Since then, it has become an efficient technique for synthesis of polymers with precisely controlled molecular architecture (topology, composition, functionality) [81-84] and for the preparation of various hybrid materials [85, 86] and bioconjugates [87, 88].

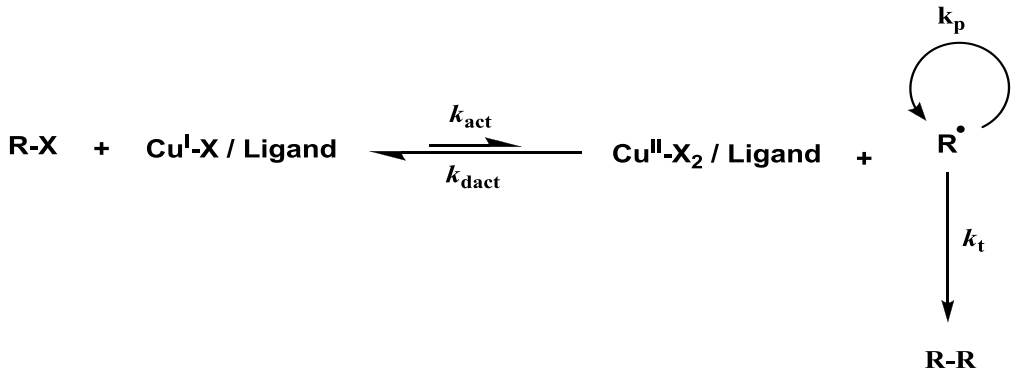

Scheme 2.1: Reaction mechanism for atom transfer radical polymerization.

ATRP is based on dynamic equilibrium between dormant and active species catalyzed by redox active transitional-metal complexes such as copper coordinated to various nitrogen based ligands [28, 79, 89]. The reaction schematic of a typical ATRP reaction is shown in Scheme 1. Radicals are formed from a dormant alkyl halide (R-X) by activation with Cu(I) species (k_{act}), after which they can either self-terminate (k_t), be

deactivated by reaction with the X-Cu(II) species (k_{deact}) or propagate in presence of a monomer (k_p). As a result of the persistent radical effect [31], the equilibrium is strongly shifted towards the dormant species ($k_{act} << k_{deact}$); thus, the radical concentration is low and termination is suppressed. The degree of control in ATRP is affected by the position of the equilibrium ($K_{ARTP} = k_{act}/k_{deact}$) and by the rate constants. K_{ATRP} depends on solvent, temperature, monomer and oxidation state of Cu species.

Despite its recognition as a preferred method for controlled polymerization [77], a disadvantage of ATRP, which limits its widespread industrial utilization or product throughput is that the transition metal complexes have to be removed from the reaction mixture and preferably recycled, [90] as high catalyst concentrations are required for ATRP. Added expense is therefore associated with purifying the generated polymer [90]. An additional problem of industrial relevance involves special handling procedures to remove all oxygen and oxidants from these systems. Previous research intending to streamline the process and products by ATRP has focused on maximizing the efficiency of catalyst removal or recycling using various methodologies such as catalyst adsorption using ion-exchange resins, extraction with water or polymer precipitation and use of solid supported catalysts [6, 18, 22, 90]. However, the most attractive approach is simply to reactivate the deactivated catalyst within the reaction system. This approach can both scavenge oxidants and decrease the amount of catalyst needed (to ppm levels), where its removal or recycling may be more easily accomplished or altogether unwarranted for many industrial applications.

Chapter 2

Matyjaszewski *et al.* have recently reported a new efficient and convenient procedure for initiating controlled polymerization reaction using activators regenerated electron transfer (ARGET) ATRP. In this system, Cu(I) complexes are regenerated from oxidatively stable Cu(II) species by the action of reducing agents within the polymerization reaction system [91]. In these systems, redox processes occur without the formation of initiating radicals, or initiating species, and therefore pure copolymers with complex architectures (e.g., block, random and star copolymers) can be formed starting with the oxidatively stable catalyst precursor complex [92].

In this chapter, ARGET ATRP of PNIPAAm in presence of air using a silane initiator, minute amount of Cu(II)/ligand complex, and FDA approved reducing agents is reported. The ARGET ATRP of PNIPAAm was carried out on initiator immobilized substrate and also in bulk aqueous solution using two types of reducing agents. A variety of complementary characterization techniques were used to study the structure, purity and thermo-responsive behavior of PNIPAAm using ellipsometry, X-ray photoelectron spectroscopy (XPS), time-of-flight secondary ion mass spectroscopy (ToF-SIMS), Fourier-transform infra-red spectroscopy (FTIR), gel permeation chromatography (GPC), goniometry and spectrophotometry. Our results demonstrated that ARGET ATRP is a significant improvement over traditional ATRP for synthesizing controlled uniform polymer brushes, since it can be carried out in ambient environments and using drastically reduced amount of the transition metal catalysts.

2.2 Experimental Section

2.2.1 Materials and preparations

N-isopropylacrylamide (NIPAAm), Cu(II)Br (98% pure), *N,N,N′,N″,N″*-pentamethyldiethylenetriamine (PMDETA, 99% pure), ascorbic acid (reagent grade, 20-200 mesh), anisole (anhydrous, 99.7% pure) and tin(II) 2-ethylhexanoate ($Sn[EH]_2$, ~95% pure) were purchased from Sigma-Aldrich (St. Louis, MO). The NIPAAm monomer was recrystallized twice in a benzene/hexane mixture and then dried under vacuum before use. The ATRP initiator (3-trimethoxysilyl) propyl 2-bromo 2-methylpropionate was ordered from Gelest and stored under dehumidified condition until used. Methanol (HPLC grade), acetone (HPLC grade), sulfuric acid (98% conc.), hydrochloric acid (98% conc.) and hydrogen peroxide were received from Honeywell Burdick & Jackson (Deer Park, TX). Poly(NIPAAm) polymer (molecular weight ~ 40,000) for spin coating was purchased from Polysciences, Inc. (Warrington, PA); regenerated cellulose dialysis tubing was purchased from Fischer Scientific (Pittsburgh, PA).

Spin coated PNIPAAm surface preparation: Silicon wafers (5 x 5 mm) were washed with 10 min intervals in dichloromethane, acetone, and then methanol in an ultrasonic cleaner and dried with nitrogen. A solvent mixture containing 35 mg of PNIPAAm, 5 mL of distilled water and 200 μL of 1 Normal HCL was prepared and 200 μL of this solution was evenly distributed on treated silicon wafer placed on a spin coater model 100 spinner (Brewer Science, Inc., Rolla MO) and spun at 2000 rpm for 60 sec [48].

SAM Immobilization: Silicon wafers were cleaned with concentrated HCl/MeOH (1:1 by vol.) for 30 min followed by concentrated H_2SO_4 for 30min. Wafers were then rinsed with copious amounts of DI water and dried with nitrogen. A self-assembled monolayer (SAM) of the initiator was attached to the silicon wafer by immersion in a 4 mM toluene solution at room temperature overnight. The wafer was then rinsed 3 times with toluene and dried in a stream of nitrogen.

2.2.2 Polymerization procedure

A 250 mL glass beaker containing the initiator grafted surface and a small stir bar was charged with 0.75 M NIPAAm monomer, 0.4 mM Cu(II)Br and 0.7 mM PMDETA dissolved in 30 mL of solvent. Addition of 8 mM reducing agent to this solvent mixture initiated the polymerization reaction which was carried out in two different ways based on the type of reducing agent used. The solvent used for the reaction is: (1) Anisole for $Sn[EH]_2$ as reducing agent; (2) DI water/MeOH (1:1 by vol.) for ascorbic acid as reducing agent. After allowing the reaction to progress at room temperature for desired polymerization time, the sample was rinsed with acetone, methanol and distilled water. The treated sample was then Soxhlet extracted at 80°C using MeOH solvent for overnight to remove any unreacted monomer and other reactants if contained on the polymer grafted surface.

The polymer synthesis in aqueous solution was carried out in a similar way using the same contents and molar proportions, but by the addition of ATRP initiator to the

solvent instead of immobilizing on to a surface. Polymerization reaction was conducted in the bulk solvent (DI water/MeOH) using ascorbic acid. After reaching a desired polymerization time, 3mL of sample was collected using a syringe and quenched with acetone to suppress the reaction followed by rotary evaporation of this mixture. The precipitate obtained was dissolved in distilled water for standard dialysis purification using methanol solvent and then again rotary evaporated and dried in a vacuum desiccators to yield a pure PNIPAAm polymer.

2.2.3 Analysis

The thickness of dry polymer brushes grafted on silicon substrates were measured using a spectroscopic ellipsometer (M-44, J.A. Wollum Co, Lincoln, Inc., NE, USA) at a wavelength range of 400-700 nm and an angle of incidence of 75°. A Cauchy model was used for the index of refraction [89] of organic layers over silicon substrate for which optical constants had been measured immediately before and after the formation of organic film.

All XPS spectra were taken on a Kratos Axis-Ultra DLD spectrometer. This instrument has a monochromatized Al Kα X-ray and low-energy electron flood gun for charge neutralization. X-ray spot size for these acquisitions was on the order of 300 x 700 μm (Kratos "Hybrid" mode). Pressure in the analytical chamber during spectral acquisition was ~5 x 10^{-9} Torr. The pass energy for survey spectra and high resolution spectra (carbon) was 80 eV and 20 eV respectively. Data treatment was performed on CasaXPS software (Manchester, UK). Core-level spectra were peak fit using the

minimum number of peaks possible to obtain random residuals. A 70% Gaussian/30% Lorentzian line shape was used to fit the peaks, and a linear function was used to model the background.

Time-of-flight secondary ion mass spectroscopy (ToF-SIMS) data was acquired with an ION-ToF ToF-SIMS 5 spectrometer using a 25 keV Bi^+ primary ion source in the pulsed mode and a reflectron time-of-flight mass analyzer for detection of the secondary ions. Both positive and negative secondary ion mass spectra were collected over a mass range from m/z = 0 to 500 and analyzed with an IonSpec data reduction software. As both the positive- and negative-ion mass spectra showed similar trends, only positive-ion ToF-SIMS spectra were presented in this study. Spectra were acquired using an analysis area of 0.01 mm^2. Positive ion spectra were calibrated using the CH_3^+, $C_2H_3^+$, $C_3H_5^+$, and $C_7H_7^+$ peaks before further analysis. The mass resolution of the secondary ions peaks in a positive-ion spectra were typically between 6000 and 9000 for m/z = 27. Three replicates were prepared for each sample type, with five spectra acquired from different locations on each replicate. ToF-SIMS positive-ion spectra from different samples types (SAM, spin coated PNIPAAm and ARGET ATRP grafted PNIPAAm) were compared using principal component analysis (PCA), which captures the linear combination of peaks that describe the majority of the variation in the dataset. PCA was performed using PLS Toolbox v.2.0 (Eigenvector Research, Manson, WA) for MATLAB (MathWorks, Inc., Natick, MA).

Chapter 2

Fourier transform infrared (FTIR) analysis was performed on a spectrometer (Nicolet 6700, Thermo Scientific) using a grazing angle reflectance tool (Smart SAGA, Thermo Scientific) and OMNIC software program (Thermo Scientific, Inc.). Grazing angle reflectance is the technique of choice for analyzing thin coatings or deposits because the high angle of incidence increases the path length of the infrared beam through the material of interest, significantly enhancing sensitivity. Monolayer sensitivity is achievable due to the high angle of incidence and selective polarization.

Gel permeation chromatography (GPC) molecular weight determination was performed using a Polymer Labs 220 PL-GPC equipped with a UV-vis detector. Two columns (PLgel 5mm MiniMIC-C, 250 X 4.6 mm) and a guard column (PLgel 5 mm MiniMIC-C, 50 X 4.6 mm) were used in series with a flow rate of 0.4 mL/min and a run pressure of 6.0 MPa. Chloroform was used as the eluent and calibration was performed using polystyrene standards with a narrow molecular weight distribution (Fluka ReadyCal 400-2,000,000).

An Advanced Goniometer model 300-UPG (ramé-hart instrument co., Mountain Lakes, NJ) with an environmental chamber and DROPimage Standard program was used to measure inverted bubble contact angles in Ultrapure water (> 18 M Ohm cm). Contact angles (θ) were taken at temperatures well above and below the solution LCST.

A UV-vis spectrophotometer (UV-1601, Shimazdu, Japan) was used to analyze the change in transmittance associated with the phase transition of PNIPAAm. The samples were dissolved in distilled water to a concentration of 1mg/mL. Samples were

placed in 4ml UV cuvettes and were subjected to a heating rate of 1°C/min from 25 to 45°C. Transmittance measurements were recorded every 30 sec. To avoid bubble formation during heating, samples were sonicated briefly prior to testing.

2.3 Results and Discussion

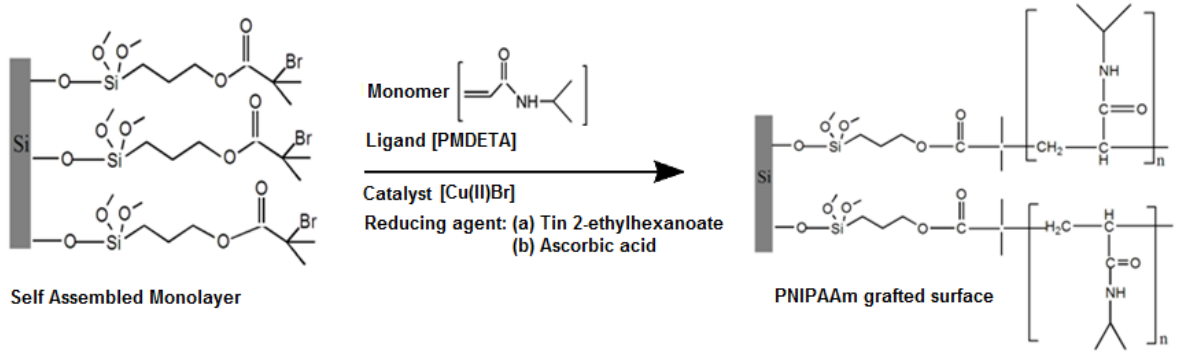

Scheme 2.2: Reaction schematic of PNIPAAm grafted on initiator immobilized silicon substrate using ARGET ATRP.

The reaction schematic for the surface polymerization of PNIPAAm is shown in Scheme 2.2. Free radical polymerization was carried out using two different reducing agents (tin(II) ethylhexanoate and ascorbic acid) separately. ARGET ARTP utilizes an excess concentration of reducing agent and much smaller concentration of copper (~50-100 ppm) to facilitate the continuous reduction of Cu(II) to corresponding copper(I) complex, which is needed to initiate the polymerization reaction by the homolytic cleavage of alkyl halide bond (R-X) of the initiator. On the other hand, the oxygen

diffusing into the solvent from ambient air continuously oxidizes Cu(I) to Cu(II) and thus, results in a controlled polymerization reaction by having only a small amount of Cu(I) complex in the solvent mixture throughout the reaction process [93-96].

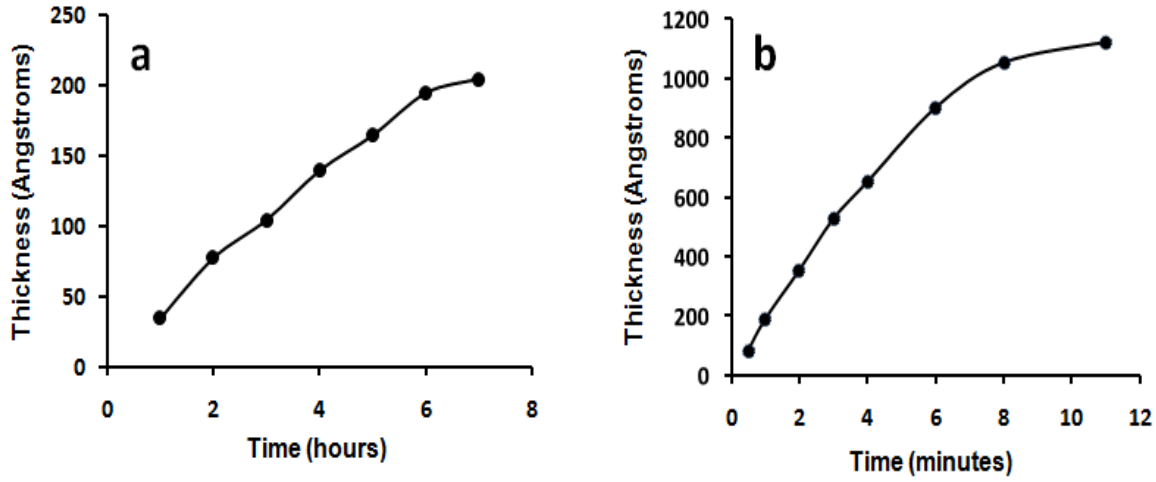

Fig. 2.2: Ellipsometry: Dry thickness of grafted PNIPAAm surface corresponding to different polymerization time measured at room temperature; (a) Synthesized using ascorbic acid as reducing agent, (b) synthesized using tin 2-ethylhexanoate as reducing agent.

The dry thickness of the polymer brush grafted on silicon substrates measured using ellipsometry is shown in Fig. 2.2. The PNIPAAm film thickness as a function of polymerization time for reaction carried out in anisole using $Sn[EH]_2$ as a reducing agent is shown in Fig. 2.2a; it follows an almost linearly increasing profile with respect to its polymerization time even after 6 hours. Fig. 2.2b illustrates the polymer brush thickness

with respect to its polymerization time for ascorbic acid as reducing agent. In this case, it is observed that the rate of grafted polymer thickness and indeed the polymerization reaction was very fast relative to Fig. 2.2a. The thickness increased linearly up to a polymerization time of 6 min and then slowed. The possible reason for this drastic variation in the rate of polymer brush growth is likely that the ascorbic acid is very stronger reducing agent and highly soluble in the solvent used relative to $Sn[EH]_2$.

The rate of monomer consumption or the rate of polymerization in ATRP depends on the absolute ratio of the concentration of activator Cu(I) and deactivator X-Cu(II) [92, 97]. Ascorbic acid, being a stronger reducing agent, results in a higher concentration of Cu(I) radical at any given polymerization time which leads to a faster rate of polymerization. On the other hand, $Sn[EH]_2$ which is a mild reducing agent with slow solubility in anisole maintains a lower concentration of Cu(I) radical leading to a relatively low but controlled reaction rate. The reason for deviation in the linearity (Fig. 2.2b) at higher polymerization time was probably due to loss of control over the reaction due to complexation of Cu(I) with excess NIPAAm present in the solvent [98, 99].

XPS was used to confirm the formation and determine the compositions of both the initiator immobilized on silicon substrate (i.e., the SAM) and the successful polymerization of PNIPAAm. As analyzed from wide-scan spectra, the surfaces are seen to consist of carbon, oxygen, silicon and bromine for SAM and carbon, oxygen and nitrogen for PNIPAAm grafted brushes (Table 2.1). A split of two Si peaks was observed in the wide-scan spectra of SAM suggesting two different types of silicon, Si and SiO.

This can be attributed to the Si signals from both the bare silicon wafer and SAM. The relative elemental composition (C/Br and C/O) of SAM surface shown in Table 2.1a confirms the SAM immobilization on the surface. The wide scan spectra of PNIPAAm brushes synthesized using $Sn[EH]_2$ and ascorbic acid showed characteristic signals attributed to carbon, nitrogen and oxygen (Fig. 2.3a and 2.3c), but PNIPAAm grafted surfaces synthesized using the $Sn[EH]_2$ reducing agent also showed a peak due to of tin (labeled Sn 3d) at a binding energy (BE) of 504.25 eV.

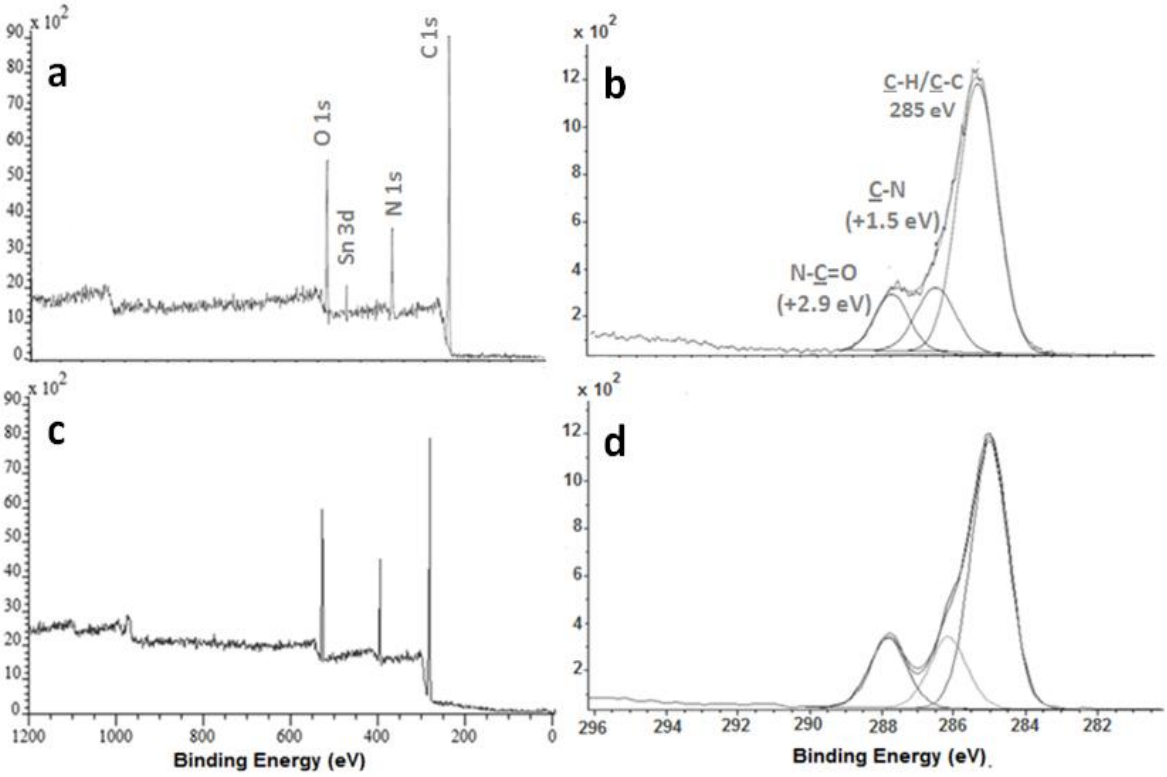

Fig. 2.3 (a, c): Wide-scan spectra of PNIPAAm grafted surfaces using tin(II) 2-ethylhexanoate (a) and ascorbic acid (c); (b, d): C1s high resolution spectra of PNIPAAm grafted surface using tin(II) 2-ethylhexanoate (b) and ascorbic acid (d).

XPS results show that traces of tin (corresponding to ~3 atomic percent) are retained on the grafted PNIPAAm surfaces when ARGET ATRP reaction is carried out using $Sn[EH]_2$ as reducing agent (Table 2.1b). It should be noted that tin is a toxic compound for marine microorganisms and is considered as problematic in terms of environmental pollution, human health and is not feasible for biomaterials which are in intimate contact with human tissue [100, 101].

The C1s resolution of PNIPAAm grafted brushed was deconvoluted by curve-fitting into three peak components (Fig. 2.3b and 2.3d): (1) the sp^3-hybridized carbon peak with a BE at 285.0 eV attributable to the aliphatic hydrocarbon (labeled C–H/C–C), (2) the peak with a BE at 286.5 eV corresponding to the –CH– unit adjacent to the –NH– group (labeled C–N), (3) the sp^2-hybridized carbon peak with a BE at 287.9 eV attributable to the amide group (labeled N–C=O). The atomic concentrations relative to the theoretical values expected for the NIPAAm compound are shown in Table 1b.

XPS spectra of PNIPAAm indicated the presence of nitrogen on PNIPAAm grafted surfaces which confirm the presence of NIPAAm (Table 2.1b and Fig. 2.3). A similar trend (Fig. 2.3(b, d)) and elemental composition (C–H, C–N and N–C=O) was observed in the high resolution spectra of PNIPAAm surfaces synthesized using $Sn[EH]_2$ and ascorbic acid reducing agents, which closely match the typical spin coated PNIPAAm surface [48], thus, further verifying the successful grafting of PNIPAAm brush. The elemental composition (Table 1b) obtained for the wide-scan spectra (Fig. 2.3(a, c)) showed on detectable amounts of Si, indicating that the PNIPAm grafted brush on the silicon substrate was >100 Å.

a	Ratio of Atomic %	Theoretical	Experimental
	C / Br	7	5.27±0.6
	C / O	1.4	1.2±0.2

b	Atomic %	Theoretical	Experimental I	Experimental II
	C	75	77±0.6	76.4±0.2
	N	12.5	10.4±0.5	12±0.2
	O	12.5	9.5±0.8	11.6±0.2
	Sn I	0	3.1±0.4	0
	C-C/C-H	66.7	70.2±8.2	61.5±4.8
	C-N	16.7	17.9±7.1	20.8±3.8
	N-C=O	16.7	11.9±1.4	17.7±1.2

Table 2.1: X-ray photoelectron spectroscopy – Experimental compositions obtained from wide scan spectra of (a) SAM and (b) PNIPAAm grafted on silicon substrate; C-C/C-H, C-N, and N-C=O represent experimental compositions acquired from high resolution C1s spectra of surface grafted PNIPAAm via ARGET ATRP using $Sn[EH]_2$ (I) and ascorbic acid (II).

ToF-SIMS and PCA analysis was used to further examine the retention and integrity of PNIPAAm brushes synthesized using ascorbic acid and to compare these with spin coated PNIPAAm surfaces. ToF-SIMS is considered to be a complementary semi-quantitative surface analysis technique as it yields information regarding molecular species at the interface with a depth resolution of 1-2 nm.

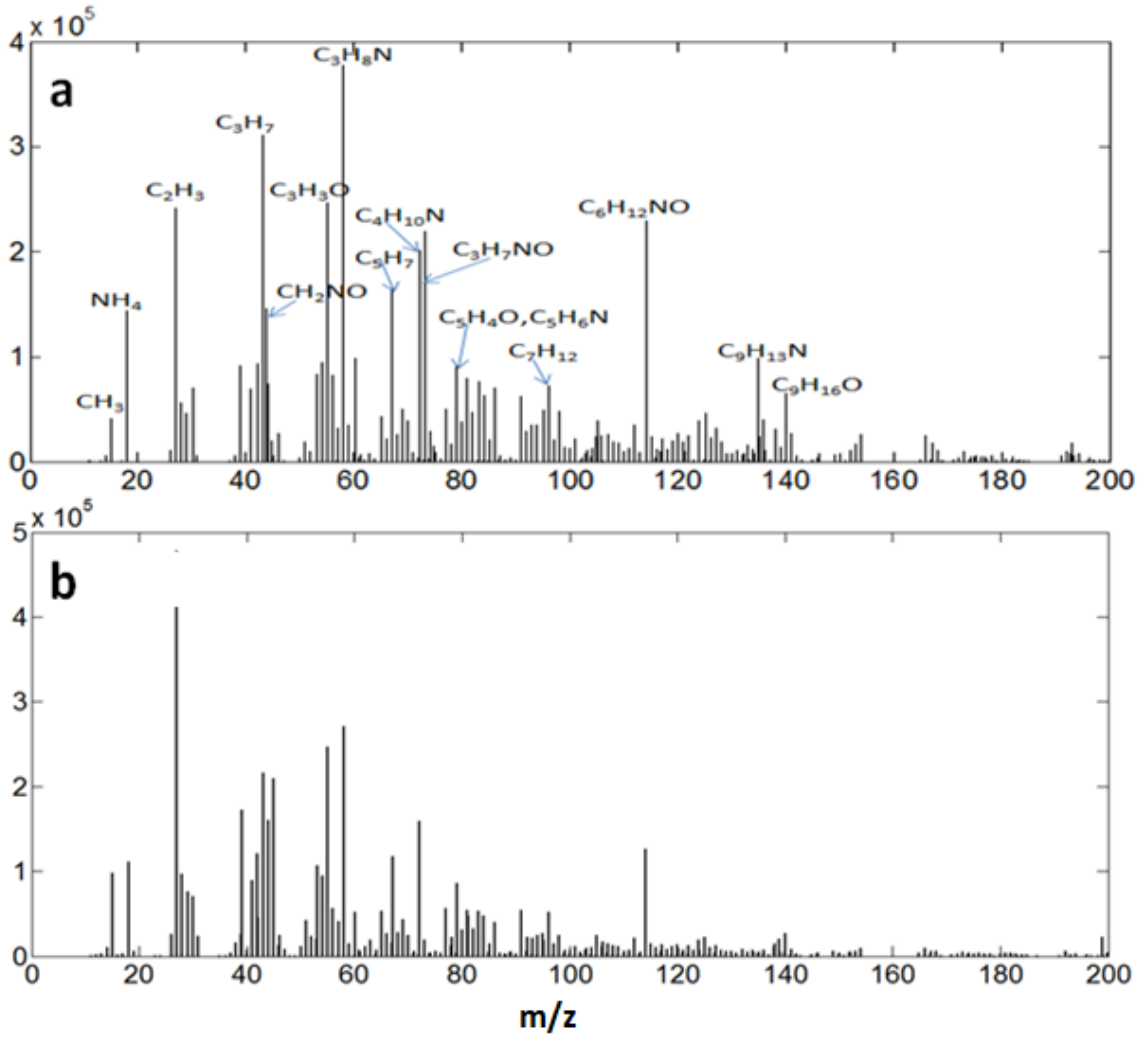

Fig. 2.4: ToF-SIMS positive ion spectra of (a) PNIPAAm brush grafted on silicon substrate and (b) Spin coated PNIPAAm on silicon substrate.

A representative ToF-SIMS positive-ion spectrum of a grafted PNIPAAm brush in the range of 0 to 200 m/z is shown in Fig. 2.4a. The spectrum shows significant signals of NIPAAm molecular fragments such as NH_4^+ (m/z = 18.0371), $C_2H_3^+$ (27.0229), $C_3H_7^+$ (43.0550), $C_3H_3O^+$ (55.0190), $C_5H_7^+$ (67.0613) and $C_3H_8NO^+$ (74.0638) [55]. Moreover,

the high intensity peaks of monomer ($C_6H_{12}NO^+$, 114.0923) and isopropyl ($C_3H_8N^+$, 58.0681) fragments clearly manifest that NIPAAm structural units of the polymer are present on the brush surface. Also, the inspection of negative-ion ToF-SIMS spectra (not shown here) did not show any characteristic signals at m/z of 71 ($C_3H_3O_2^-$) and 72 ($C_2O_3^-$) that are associated with ascorbic acid, thereby confirming the absence of any detectable traces of ascorbic acid on the polymer brush grafted surfaces using. We also compared the positive-ion spectra of ATRP grafted surfaces with spin-coated PNIPAAm (Fig. 2.4b) surfaces which also contained most of these characteristic peaks.

ToF-SIMS is an energetic process which yields hundreds of peaks in the 0-200 m/z range, making the interpretation of spectra difficult, especially when spectra acquired from different treatment methods are compared. Principal component analysis (PCA) is used to aid the interpretation of spectra by indentifying related variables and focusing on the differences between the spectra [102, 103]. Figure 2.5a represents the scores plot of principal component 2 (PC 2), versus principal component 3 (PC 3). Examination of Fig. 2.5a shows that majority of mass fragments from each type of sample aggregate separately; all nominal mass fragments (●) from the ARGET ARTP grafted PNPAAm sample are grouped within the negative-x and -y quadrant, SAM m/z fragments (Δ) are aggregated towards the horizontal x-axis within positive-x and positive/negative-y quadrants and the spin-coated PNIPAAm sample fragments (+) are spread within the negative-x and positive-y quadrant. To better percept the reason for these differences, we must inspect the loading plot for each PC.

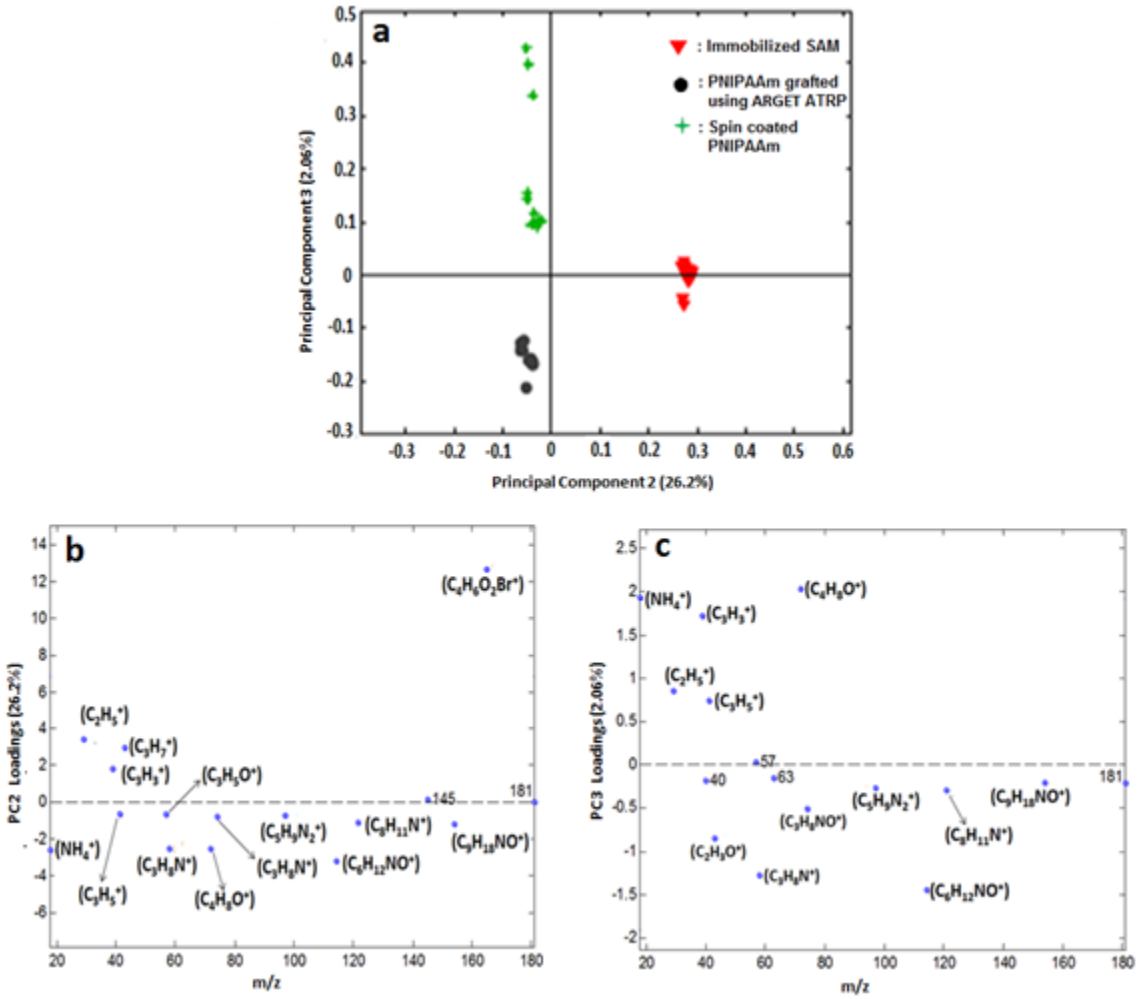

Fig. 2.5: PCA of positive ToF-SIMS including (a) scores plot for PC3 versus PC2, (b) PC2 loading plot and (c) PC3 loading plot.

Figure 2.5b represents the loading from PC 2. Each of the peaks in the PC 2 loading plot (Fig. 2.5b) below the origin corresponds to samples in the scores plot (Fig. 2.5a) that load negatively and each of the peaks above the origin in the PC 2 loading plot corresponds to samples in the scores plot that load positively. By comparing the PC 2

loading plot to the scores plot, we find that the PNIPAAm sample (●) peaks such as $C_3H_8N^+$ (m/z = 58.0681), $C_3H_8NO^+$ (74.0638) and NH_4^+ (18.0371) and $C_6H_{12}NO^+$ (114.0923) correspond to PNIPAAm fragments. Also, the SAM samples (Δ) are correlated with peaks originating from initiator immobilized surface, such as $C_4H_6O_2Br^+$ (m/z = 165.9938) thus clearly separating the SAMs from the PNIPAAm samples.

To understand how spin-coated PNIPAAM samples vary from grafted samples prepared using ARGET ATRP, we must examine Fig. 2.5c, the loading from PC3. By comparing the PC 3 loading plot to the PC 3 scores, we find that most of the monomer ($C_6H_{12}NO^+$, 114.0923) and isopropyl ($C_3H_8N^+$, 58.0681) m/z fragments are identified to be originating from ATRP grafted PNIPAAm samples (●). On the other hand, smaller m/z NIPAAm fragments such as $C_3H_3^+$ (m/z = 39.0228) and $C_2H_5^+$ (29.0392) corresponds to the spin-coated PNIPAAm sample. The smaller mass fragments as observed in loading plot (Fig. 2.5b) and its unconfined spread as seen in scores plot(Fig. 2.5a) for the spin-coated samples is because of the entangling of the polymer coating with difference in the polymer structure from sample to sample. Thus, ToF-SIMS mass fragments identified for ARGET ATRP samples confirm that majority of the monomer units remain structurally intact without cross-linking or any kind of impurities on grafted PNIPAAm surfaces. Also, from the scores plot (Fig. 2.5a), it clearly indicates that all m/z (●) from PNIPAAm replicates are scattered very close to each other confirming the reproducibility of exactly identical PNIPAAm grafted surfaces using ARGET ATRP.

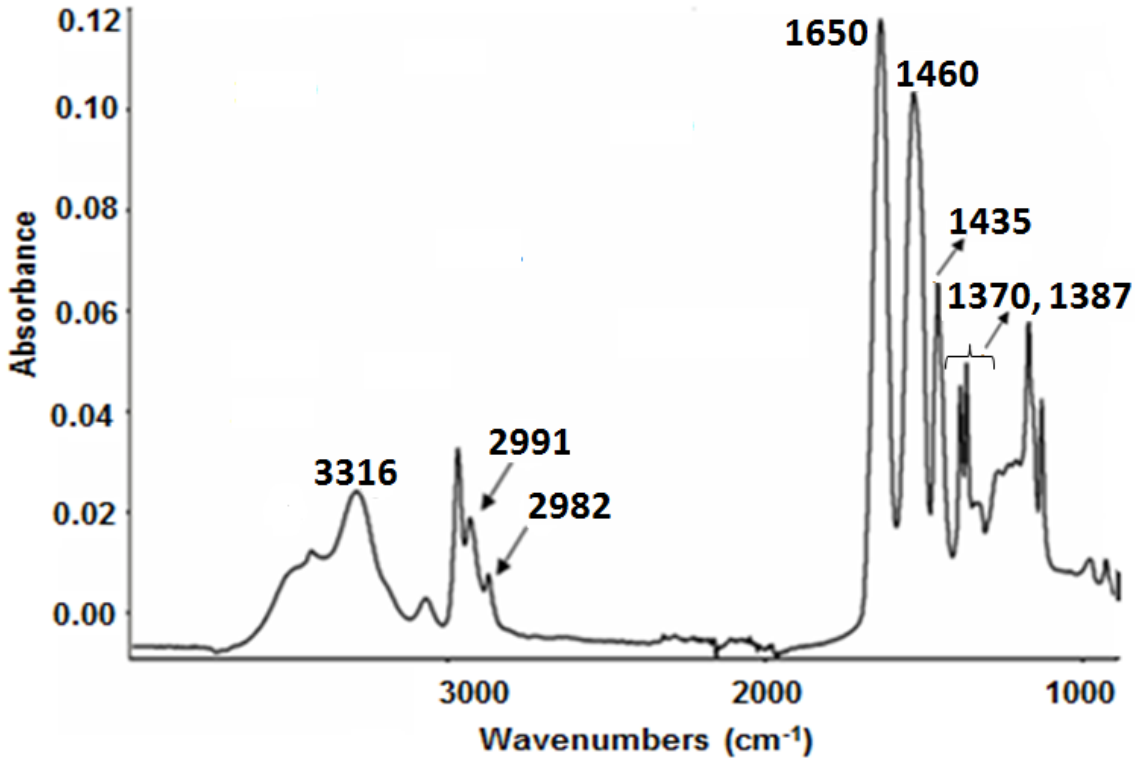

Fig. 2.6: FTIR of PNIPAAm grafted on silicon wafer using ascorbic acid reducing agent via ARGET ATRP.

The FTIR absorbance spectrum of grafted PNIPAAm brush on silicon wafer (polymer thickness of 250 Å) synthesized via ARGET ATRP using the ascorbic acid reducing agent is shown in Fig. 2.6. The absorbance peak at 3316 cm^{-1} corresponds to the N–H stretch of the NIPAAm; the peaks at 2982 cm^{-1} and 2991 cm^{-1} are attributed to the asymmetric stretching of $–C(CH_3)_2$ and $–CH_2–$ respectively. The intensive peak at 1650 cm^{-1} corresponds to the C=O (carboxyl) group, the absorbance at 1460 and 1435 cm^{-1} is due to symmetric deformation of N–H and $–C(CH_3)_2$ and the characteristic doublet at 1387 and 1370 cm^{-1} is due to the skeletal vibration stretching of isopropyl group of the

NIPAAm monomer units [104]. The presence of absorbance peaks corresponding to NIPAAm functional groups especially, the absorbance due to carboxylic and amide groups qualitatively confirms the presence of grafted PNIPAAm brush on the surface.

Polymerization time (min)	M_n (gm/mol)	PDI (gm/mol)
0.5	14052	1.0353
1	39116	1.0828
2	63211	1.1573
4	98015	1.1701
8	141225	1.2569

Table 2.2: Molecular weight and polydispersity index of PNIPAAm synthesized via ARGET ATRP using ascorbic acid with different polymerization time periods.

GPC analysis was used to examine the molecular weight distribution of PNIPAAm obtained from the fast polymerization reaction observed when ascorbic acid was used as reducing agent. Table 2.2 provides the molecular weight and polydispersity of PNIPAAm synthesized via polymerization in solution using ARGET ATRP. It clearly shows the increase in molecular weight with polymerization time along with slow, but steady increase in polydispersity index (PDI). Nevertheless, it can be observed that the

polydispersities remain close to unity indicating a controlled polymerization reaction even in the absence of deoxygenated environments.

One of the proposed limitations in the synthesis of high molecular weight polymers by ATRP is due to the side reaction by Cu(II) species during the polymerization reaction, for example, the oxidation of polystyryl radical to a carbocation by the Cu(II) species during the ATRP of polystyrene [105]. Since ARGET ATRP can be successfully carried out with small amounts of Cu(II) species, it is more feasible for the synthesis of high molecular weight polymers.

However, the molecular weight distribution curves for polymers synthesized using ascorbic acid, showed eventual appearance of shoulder peaks for a polymerization time beyond 9 minutes resulting in increased PDI, which indicates the formation of dead chains by termination reactions. The reasons for this increased PDI at higher polymerization time can also explain the slow growth of grafted polymer brush observed at higher polymerization time (Fig. 2.2b).

The thermo responsive behavior of grafted PNIPAAm surface and PNIPAAm synthesized in solution was examined using contact angle measurement (goniometry) and turbidity measurements (UV-VIS spectrophotometry). All the contact angle (θ) measurements were done using captive-bubble method [106] and the average θ was calculated from measurements taken over five replicates of same thickness. The average contact angle (θ) of PNIPAAm surface (thickness of 150 Å) grafted on silicon wafer was $28 \pm 0.2°$ when it was measured at 45°C and $47 \pm 0.9°$ when measured at 22°C. This difference in the contact angles measurements is due to the different surface wettability

of PNIPAAm brush above and below its LCST. Grafted PNIPAAm brushes exhibits a reversible change in its surface hydration properties from a hydrophilic state to a relative hydrophobic state by varying it temperature from below to above its LCST (~32°C). Below its LCST (< 32°C), the PNIPAAm brush is hydrophilic and results in a lower contact angle, whereas at temperature above the LCST (>32°C) the polymer brush is hydrophobic and there by a higher contact angle is observed. Thus, the difference in contact angles measurement above and below the LCST, verifies the thermo responsive behavior of PNIPAAm grafted surfaces synthesized using ARGET ATRP.

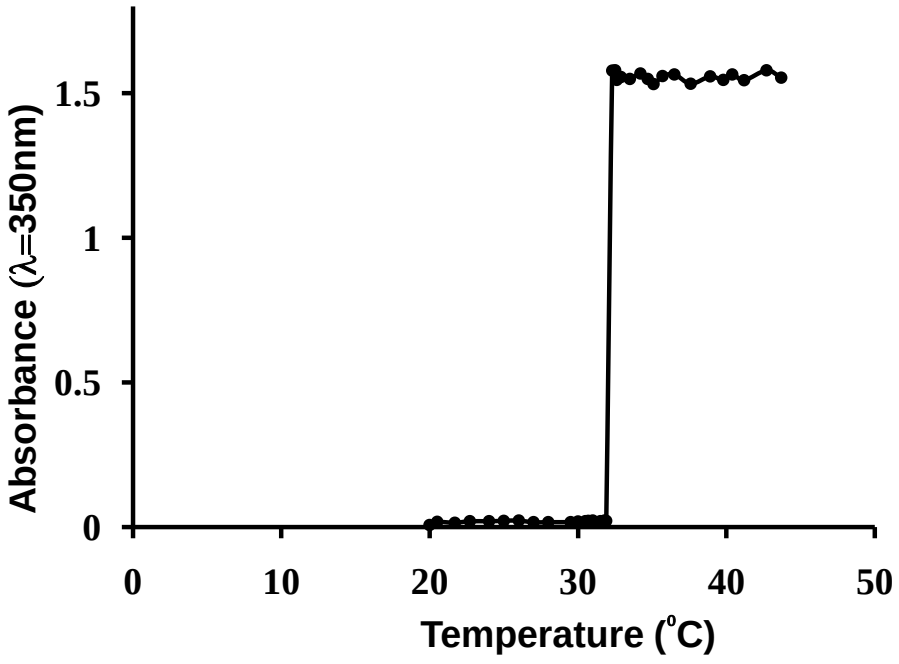

Fig. 2.7: Turbidity curve obtained using UV-Vis absorption spectrophotometry for PNIPAAm synthesized in aqueous phase synthesized using ATRP.

The turbidity curve shown in Fig. 2.7 was measured by following a step-wise increase of the polymer solution temperature in the range from 20 - 45°C. The intensity of relative absorbance shows a sudden increase at ~32°C indicating a change in the UV light transmittance of spectrophotometer near to the LCST of PNIPAAm. At temperatures below 32°C the polymer is completely soluble in the aqueous solution and therefore results in negligible absorbance of the UV light, but when the temperature of the solution reaches ~32°C, PNIPAAm undergoes a phase transformation from a transparent liquid to a milky white, opaque gel which results in a relative high absorbance. This transition is presumably due to the collapsed polymer chains [107] in aqueous solution at temperatures well above the LCST of PNIPAAm and thus exhibits a thermo responsive behavior.

All the above performed different surface analysis techniques indicate that using ARGET ATRP well defined PNIPAAm polymers can synthesized both on grafted surfaces and in aqueous solution with reversible change in hydrophobicity above and below its transition temperature. Hydrophobicity appears to play a role in maintaining cellular attachment. Prior studies have shown that, although some cells may initially attach well to hydrophobic surfaces, they are easily removed upon application of low shear forces for polymers [108]. Our group has previously demonstrated the ability of the temperature responsive PNIPAAm polymer to reversibly attach and release bacteria when grafted on to a surface [51, 52]. These materials have been shown to release not only newly attached bacteria (i.e., at 2 h), but also fully developed biofilms (i.e., at 72 h) [52].

For release to occur, however, the surface transition must be from one favored for attachment to one disfavored. For example, from our previous studies, *Cobetia marina*, which attaches in greater numbers to surfaces with a higher water contact angle [108, 109], attaches well to PNIPAAm surfaces above its transition temperature (>32°C); when rinsed with solutions below 32°C, *C. marina* is released from the surface [51, 52]. The reverse, i.e., attaching *C. marina* below LCST and rinsing above 32°C, results in no significant release of cells from PNIPAAm surfaces [52]. However, these studies were performed at lower shear forces (i.e., ordinary rinsing) and the cell detachment under an applied larger shear forces are somewhat still poorly understood. In our next step, we propose to develop a quantitative technique for studying the detachment of cells under an applied known larger shear forces.

Chapter 3

Thermo-Responsive Polymers for Quantitative Cell Adhesion Studies Using Spinning Disk Apparatus

3.1 Introduction:

Many different types of bacteria attach to a wide range of solid surfaces, and bacterial attachment to surfaces often has a significant effect on their ecology, physiology and behavior. Bacterial adhesion to a solid surface is a critical step in the process of biofilm formation. These biofilms as introduced in chapter 1 are in turn, the common cause of biofouling occurring in an extremely wide range of situations, from the colonization of medical devices to the production of ultra-pure, drinking and process water and the fouling of ship hulls, pipelines and reservoirs. It is a subject which has attracted much investigation by microbiologists, physical chemists, material scientists and civil engineers [110]. As bacteria move toward a solid surface, the initial interaction between the cell and the surface is governed by long and medium range forces, primarily vander Waal and electrostatic forces [111, 112]. These forces depend on the physicochemical properties of substratum and the bacterial surface, such as hydrophobicity [113], free energy [114] and surface charge [113] .

Chapter 3

Understanding the phenomena of adhesion and detachment of micro-organisms and biofilm from surfaces provides a better understanding of cell-surface interactions and is an extremely important factor for reducing biofouling. McKeever *et al* [115] investigated adhesion strength of eukaryotic cells using micromanipulation which involves pulling of a cell from surface using micropipette. Cao *et al.* [116] and Fallman *et al.* [117] measured detachment forces using atomic force microscopy and optical tweezers to quantify tip-cell interaction force and surface elasticity. Another approach used by Walker et al. [118] and Meinder *et al.* [119] involved DLVO theory (named after Derjaguin, Landau, Verwey and Overbeek) in which binding strength between micro-organisms was calculated based on the basis of Liftshitz-Vander Waals (acid-base and), electrical double layer interactions. Although extensive studies on the subject of detachment of cell from substrate have been made experimentally and using mathematical modeling, the quantitative mechanical aspects of adhesion remain poorly understood because of a lack or robust, quantitative measurement systems, and the inherent complexities of the adhesion process.

Fluid flow is an important factor in microbial adhesion and detachment from surfaces [120]. An increase in fluid flow velocity will in the first instance yield increased microbial transport towards a substratum surface (convective diffusion), but at the same time causes an increase in hydrodynamic detachment forces. Shear is the dominant effect of fluid flow on surfaces and can be well controlled in experimental systems, such as in rotating disk [121] and flow cell [122]. A significant feature of rotating or spinning disk system is the application of detachment forces under constant and uniform surface

chemical conditions [123]. Since surface-active materials react with surrounding fluids, investigation of the effects of the chemical environment on cell adhesion is important in the analysis of cell detachment to these substrates.

We have reported earlier that thermo responsive PNIPAAm surfaces can mediate reversible attachment/detachment of prokaryotic cells and thus can be used as a novel approach for reducing biofouling [46, 49, 51, 53]. LCST (~ 32°C) mediated transition of surface-grafted PNIPAAm homopolymer materials results in reversible changes in the number of adherent bacteria (*Staphylococcus epidermidis and Halomonas marina*) dependent on the inherent preferences of these bacterial strains for hydrophilic or hydrophobic substrates [52]. Thus, following our previous investigations the objectives of the present study include: (1) to propose a novel methodology, using a spinning disk apparatus, to quantitative study the effect of shear force on the detachment of marine biofouling bacteria from grafted PNIPAAm surfaces, (2) to correlate the behavior of bacterial detachment profiles from PNIPAAm grafted surface under shear environment and at temperature well above and below the LCST, and (3) to investigate the effect of time period of incubation and thickness of PNIPAAm brushes on the cell detachment under the action of a reproducible know shear forces.

3.1.1 Description of spinning disk

Spinning disk apparatus as shown in Scheme 3.1 consists of a fluid-filled bath in which a disk containing the sample substrate is submerged. The sample and disk are connected to a drive shaft protruding into the fluid bath. The rotation of the disk is driven

by a motor with its speed controlled by an optical sensor which is connected to a tachometer [124]. A system of top and side baffles is used to minimize rotation of the bulk fluid. Dimensions critical to achieve laminar flow patterns have been highlighted in the schematic. The spinning disk configuration has been extensively studied [125, 126] and the flow patterns and mass transport have been characterized precisely through electrochemical measurements [123, 127].

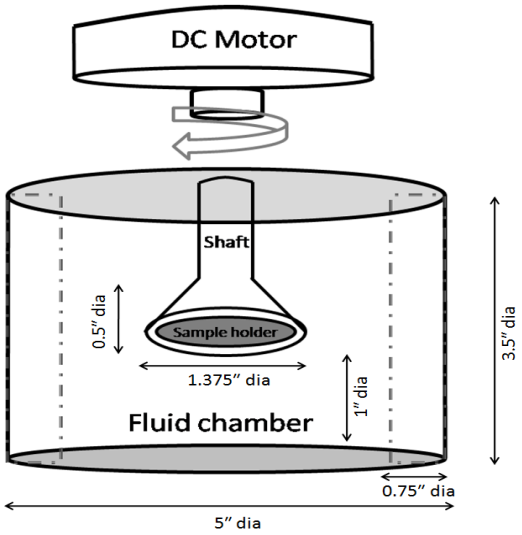

Scheme 3.1: Schematic of spinning disk apparatus used for cell adhesion strength measurements.

The rotation of the disk draws in fluid axially from its surrounding; the fluid layer near the disk is carried by it through friction and attains a rotational speed which is compensated by flow of fluid in the axial direction towards the disk which in turn carried and ejected centrifugally. The centrifugal force per unit volume acting on a fluid particle at the rotating disk surface is proportional to its radial position from the center of the

disk. Thus, the spinning disk applies force that varies with the radial position on the sample.

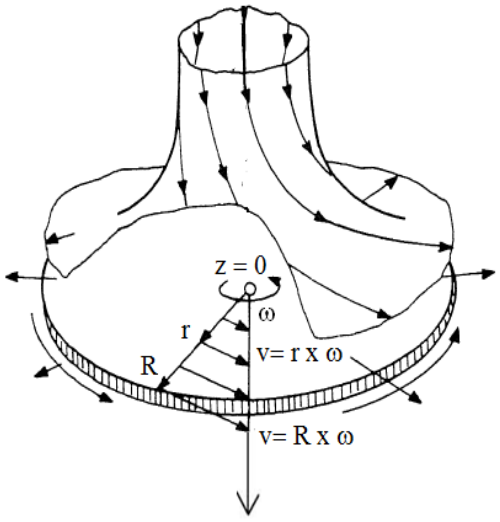

Scheme 3.2: Velocity profile of the fluid near the surface of a rotating disk [126].

Velocity distribution and shear forces: The velocity profile of the fluid near the disk surface is shown in Scheme 3.2. It represents a three-dimensional flow i.e. it exhibits velocity components in radial (r), circumferential (φ), and axial directions (z) denoted by ϑ_r, ϑ_φ and ϑ_z respectively. The motion of the fluid gives rise to shear stress components in each of these directions given by $\tau_r, \tau_\varphi, \tau_z$ (τ_z = 0 at the disk surface as no fluid is flowing through the surface). The velocity distribution and shear forces are obtained by solving the Navier-Stokes equation (eq. 2) along with the continuity equation (eq. 3) in cylindrical coordinates by assuming a disk of infinite radius.

Navier-Stokes equation:

$$-\Delta p + \mu\nabla^2\vartheta + \rho g = 0 \qquad \text{eq. (2)}$$

Continuity equation:

$$\Delta \cdot \vartheta = 0 \qquad \text{where, } \Delta = \frac{\partial^2}{\partial r^2} + \frac{1}{r}\frac{\partial}{\partial \varphi} + \frac{\partial^2}{\partial z^2} \qquad \text{eq. (3)}$$

Boundary conditions:

$$\text{At} \quad z = 0 \quad \rightarrow \quad \vartheta_r = 0, \quad \vartheta_\varphi = \omega r, \quad \vartheta_z = 0$$

$$\text{At} \quad z = \infty \quad \rightarrow \quad \vartheta_r = 0, \quad \vartheta_\varphi = 0, \quad \vartheta_z = -U$$

where, U is obtained from the solution itself.

Here, because of the axial symmetry all derivatives with respect to the angle φ vanish and the pressure in the fluid may be considered as constant along the radius; from the analytical solution for velocity profiles [128], the shear stress on the surface of the disk is given by:

$$\tau_{r_{z=0}} = -\mu\left(\frac{\delta\vartheta_r}{\delta z}\right)_{z=0} = -0.510\mu r\sqrt{\left(\frac{\omega^3\rho}{\mu}\right)}$$

$$\tau_{\varphi_{z=0}} = -\mu\left(\frac{\delta\vartheta_\varphi}{\delta z}\right)_{z=0} = +0.616\mu r\sqrt{\left(\frac{\omega^3\rho}{\mu}\right)}$$

$$\boldsymbol{\tau_s = \sqrt{\tau_r^2 + \tau_\varphi^2} = 0.8 r\sqrt{\mu\rho\omega^3}} \qquad \text{eq. (4)}$$

where, τ_s is the shear force acting at the surface of the disk.

3.2 Materials and Methods

3.2.1 Media and buffers

The media and buffers were prepared using ultrapure water (Synergy Ultrapure Water Systems, Millipore, Inc.). The final resistivity of the processed water was 18.4 $M\Omega cm^{-1}$. Marine Broth 2261 (MB, Difco) was prepared according to the manufacturer's instructions. Marine Agar (MA) was prepared by the addition of 1.5% Bacto agar (Difco) to MB. Artificial seawater (ASW) contains 400 mM NaCl, 100 mM $MgSO_4.7H_2O$, 20 mM KCl, 10 mM $CaCl_2$ [129]. Modified basic marine medium plus glycerol (MBMMG) contained 0.5 x ASW plus 19mM NH_4Cl, 0.33 mM K_2HPO_4, 0.1 mM $FeSO_4.7H_2O$, 10 mM trishydroxyaminomethane hydrochloride (pH 7), and 2mM glycerol [49, 52, 129].

3.2.2 Bacterial strains

Cobetia marina (*basonym, Halomonas marina*) [130-132] ATCC 25374 was revived from the original lyophilate and stored as frozen stock aliquots in MB + 20% glycerol at -70°C. Experimental stock cultures were maintained on MA slants and were stored at 22°C for 24 hours. Prior to inoculation into a chemostat, a single colony from a MB slant was inoculated into 25 ml of MB and grown overnight with shaking at 25°C. A chemostat culture was established by inoculating 3 ml of the overnight culture into MBMMG. The chemostat was maintained at a flow rate of 1 ml min^{-1} (dilution rate, 0.16 h^{-1}) with constant stirring. The concentration of the chemostat culture was ~ 10^7 cells ml^{-1} [49].

3.2.3 Density and viscosity measurements

An Ostwald viscometer (Cole-Parmer Scientific Inst.) was used to measure the kinematic viscosity of ASW at 37°C, 22°C, and 4°C. The average proportionality constant value of the viscometer used is 0.0021 cSt/s. The change in density of ASW with temperature has been published previously [133]. The calculated kinematic viscosity values and obtained density values at 37°C, 22°C, and 4°C were used to calculate the dynamic viscosity of ASW.

3.3 Experimental and Analysis methods

3.3.1 Sample preparation

Circular glass cover slips (25 mm diameter, thickness No. 2, VWR) were treated with Piranha solution for overnight followed by rinsing with distilled water and dried with nitrogen to yield uniform hydroxyl groups on the sample substrate verified by contact angle measurements ($\theta < 5°$). The hydroxylated samples were subjected to SAM immobilization using ATRP initiator and subsequently followed by ARGET ATRP of PNPAAm using ascorbic acid which is described in detail previously (chapter 2). The PNIPAAm grafted on cover slips were analyzed for its surface elemental composition and contact angle measurements using XPS (Kratos Axis Ultra Spectrometer, using Al Kα X-ray source) and goniometer (Model 300-UPG, Ramé-Hart instrument co., Mountain Lakes, NJ, USA).

3.3.2 Experimental procedure

The step-wise protocol followed for bacterial cell detachment using spinning disk apparatus is described as follows:

1) PNIPAAm grafted on glass cover slip was mounted on the sample holder of the spinning disk and immersed in pre-equilibrated (37°C) beaker with 30 mL of ASW containing *C. marina*, collected from chemostat. The samples were incubated for a pre-selected time, maintaining the constant temperature of 37°C using a temperature controlled heat plate.
2) The disk along with the shaft was immersed into the cylindrical chamber of the spinning disk apparatus which is filled with buffer (ASW) of known density and viscosity while maintaining the constant temperature (22°C).
3) The motor was started and ramped up to the pre-selected desired speed over 30 sec. Spun at a constant speed for 29 min and then decelerated back to zero over 30 sec (total spin cycle 30 min).
4) The rotating shaft and the spinning disk was removed from the fluid chamber and inverted to the upright position.
5) The vacuum was released on the back side and replaced by air flow line to facilitate removal of the sample. The sample was then transferred into a petri-dish and allowed to dry.
6) The dried sample was placed on an optical microscope (Zeiss, Carl Zeiss Microimaging, Inc., USA) sample stage along with a template (Note 1). The template helps in taking the image at known radial distance from center of the sample.

Note 1: The template used was fabricated from circular brown flexible plastic (25 mm dia.) material on which a number of square-openings (1 mm^2) across various known radial positions were made using a computer-controlled X-Y knife plotter (Graph tec FC7000-75, Western Graph tec Inc., Irvine, CA) which incorporates a knife in place of traditional ink pen [134, 135].

7) Using a focused 40X objective and the template, a minimum number of possible images were captured covering the whole of each $1mm^2$ sample surface area at various known radial distances from the center using a CCD camera (Axiocam, Carl Zeiss, Inc., USA).
8) The data transfer to computer was done using Axiovision software. Later image J software was used in counting or measuring the cell densities [136, 137].
9) The same procedure as describe above was followed for spinning disk experiments performed using samples of 190 and 900 Å polymer brush thickness and also at different constant temperatures of 37°C and 4°C in warm room and cold room respectively (Note 2).

Note 2: For each run of the spinning disk apparatus, autoclaved buffer (ASW), fresh *C. marina* culture collected from the chemostat and a new PNIPAAm grafted sample was used.

3.4 Results:

XPS wide scan spectra showed peaks of carbon, oxygen and nitrogen with atomic percentages of 73.4 %, 12.1 % and 12.2 %, respectively, calculated from the sensitivity

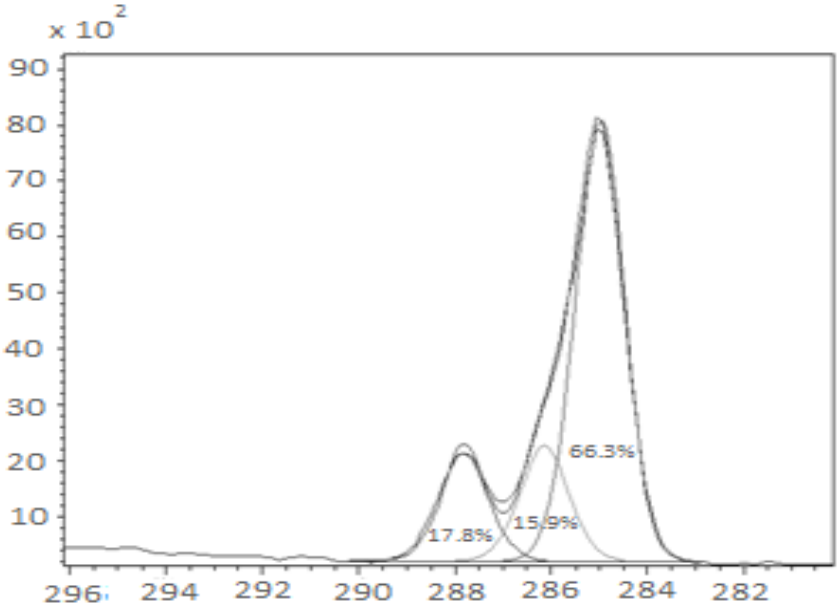

Fig. 3.1: X-ray photoelectron spectroscopy (XPS) - C1s high resolution of PNIPAAm grafted on glass substrate via ARGET ATRP deconvoluted into three peaks: C-C/C-H (66.3%), C-N (15.9%), N-C=O (17.8%).

factor-corrected area under each peak. The C1s spectrum (Fig. 3.1) resolved in to three components indicated C–H/C–C (285.0 eV), C–N (286.5 eV) and N–C=O (287.9 eV) peaks with 66.3, 17.8 and 15.9 atomic percentages. The elemental composition results obtained from both the wide scan and C1s spectra were consistent with the XPS results obtained for PNIPAAm grafted on silicon substrates (chapter 2). Contact angle (θ) measurements were obtained using captive bubble method using goniometry [106]. The average θ of PNIPAAm grafted surfaces on glass substrates with polymer brush thickness of 190±1.9 nm was 30±1° at 22°C and 47±7° at 37°C confirming the thermo-responsive behavior of PNIPAAm.

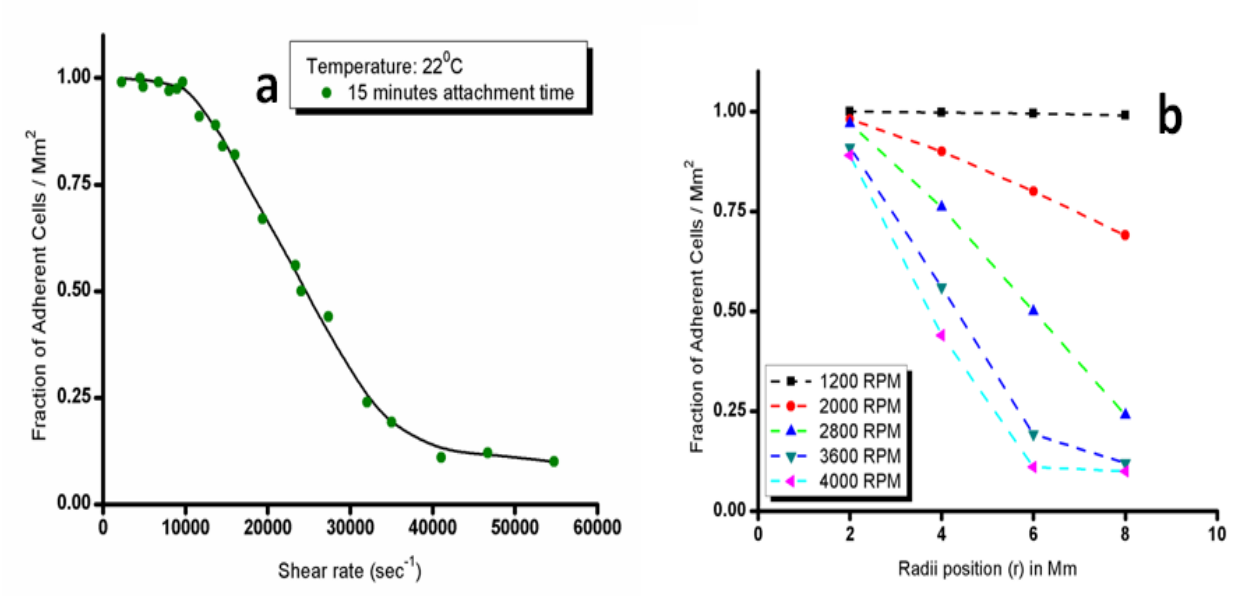

Fig. 3.2: (a) Effect of shear on cell detachment from PNIPAAm grafted surface (polymer brush thickness – 19 nm) below the LCST of PNIPAAm; (b) Fraction of adherent cells as a function of distances from the center of the sample surface.

Fig. 3.2a illustrates the fraction of adherent cells per mm^2 as a function of applied shear rate using the spinning disk device. The varying range of shear rate applied was obtained by running the spinning disk at various rotational speeds of 1200, 2000, 2800 and 4000 rpm. The fraction of adherent cells at any given radial position is calculated by normalization of measured cell densities to the cell density at the center of the sample disk (i.e., $r = 0$) where there is no shear force (τ) acting. The cell attachment or sample incubation was done for 15 minutes at 37°C, followed by bacterial detachment under shear at 22°C. Fig. 3.2a shows that almost insignificant fractional release of *C. marina* was observed below an applied shear force of approximately 100 dyne/cm^2, after which it

follows a non-linear cell detachment profile with respect to shear rate, with a small fraction (~0.1) of cells remaining adhered to the PNIPAAm brush even under higher shear force. This indicates that by changing the temperature from 37°C (incubation temperature) to 22°C and under applied known shear nearly 90% of cell release can be attained. Fig. 3.2b illustrates the fraction of adherent cells per mm^2 at any given fixed radii from the center of the sample which correlates to the shear rates applied (Fig. 3.2a).

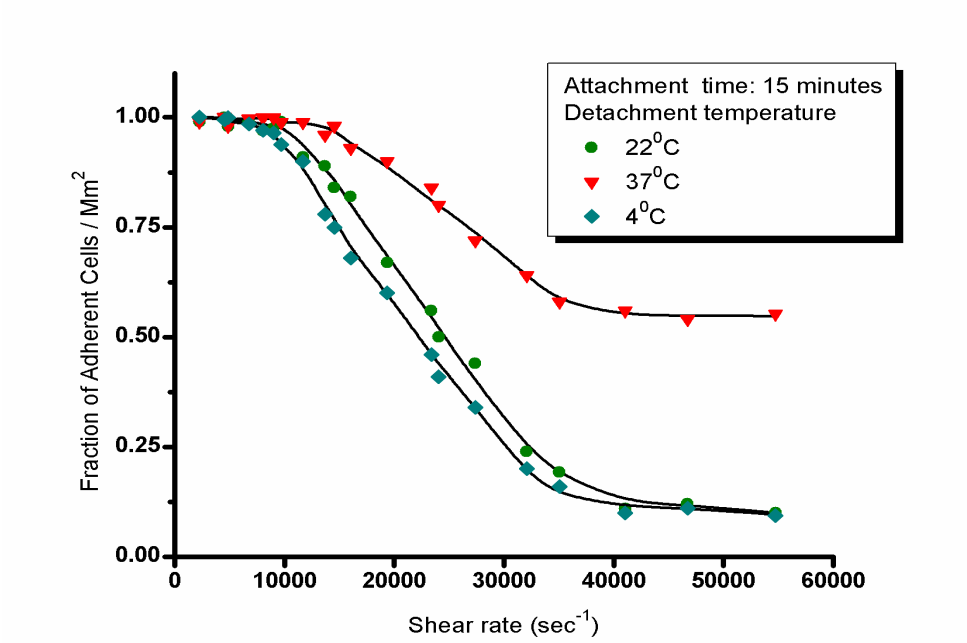

Fig. 3.3: Fraction of adherent cells on grafted PNIPAAm surface (polymer brush thickness – 19nm) under shear analyzed using spinning disk apparatus both above and below the LCST of PNIPAAm.

Fig. 3.3 shows the effect of temperature on the bacterial cell detachment under shear. It demonstrates that the spinning disk experiments performed at 22°C and 4°C showed nearly 90% of cell release from the surfaces, indicating similar cell detachment profile at temperatures well below the LCST of PNIPAAm. In contrast to this, bacteria

detachment at 37°C showed a fractional cell detachment of only up to 45% with increasing shear rate. After reaching the shear rate of 35,000 sec^{-1} the cell detachment curve followed a constant profile with increasing shear rate indicating no significant cell release. The difference is the detachment profile for experiments conducted at different temperatures is caused by the different conformation degree of surface hydration exhibited by PNIPAAm well above and below its LCST.

Fig. 3.4a and 3.4b indicate that both polymer brush thickness and time period of bacterial cell attachment affect the efficiency of cell release from thermally responsive surfaces. The polymer grafted surface with a dry thickness of 19 nm and a cell attachment time period (incubation time) of 15 minutes yielded 45% of fractional cells release after spinning for 30 minutes at 37°C (Fig. 3.4a), but when the time period of attachment (incubation) was increased to 2 hours almost negligible fraction of cell release was observed even under an applied shear rate of 50,000 sec^{-1} (Fig. 3.4b). Fig. 3.4a also illustrate that in contrast to 90% fractional cell release at 4°C from grafted PNIPAAm surface with dry film thickness of 19nm, only 35% fractional cell release was observed from a relatively thick (90 nm) PNIPAAm brush surface even under an applied shear rate of 50,000 sec^{-1}. Similarly, significant differences in cell detachment profiles were observed from experiments conducted at 4°C with different incubation time and 37°C with varied PNIPAAm polymer thickness as shown in the figures.

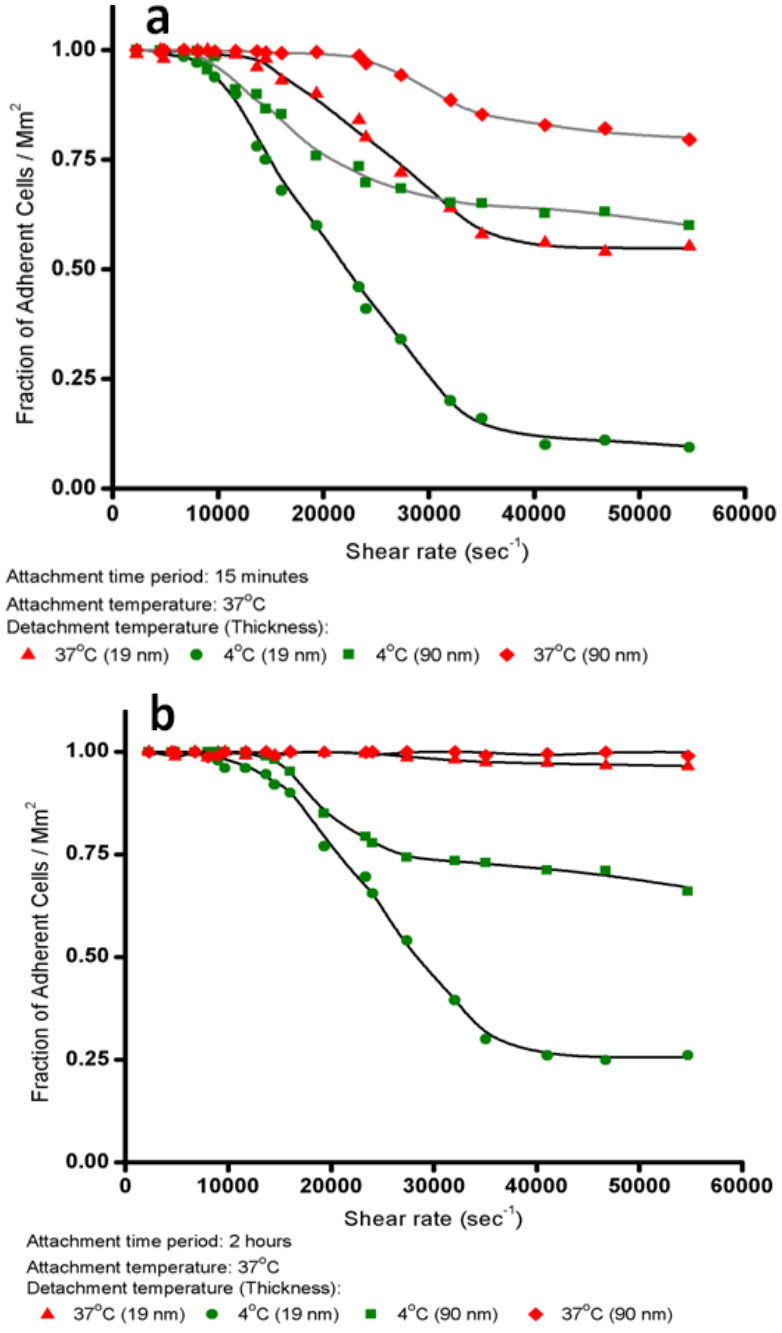

Fig. 3.4: Fraction of adherent cells as a function of shear rate applied both above and below LCST on PNIPAAm grafted surfaces having different dry polymer thickness (19 nm and 90 nm) and different cell incubation time period: (a) 15 minutes; (b) 2 hours.

3.5 Discussion:

The wide scan spectra and the peaks resolved from C1s spectra yielded elemental composition ratios for C: N: O and C–H/C–C: C–N: N–C=O as 6.1: 1: 1 and 4.2: 1.1: 1 which are consistent with the theoretical expected atomic percentages of 6: 1: 1 and 4: 1: 1 respectively. The above consistency and also the comparison of this atomic ratios with the results obtained in chapter 2 for polymer grafted on Si substrate provide convincing evidence of PNIPAAm grafted on glass with no detectable impurities. The average contact angle measurement on the PNIPAAm grafted brush measured at 22°C (below the LCST) is lower than the contact angle measured at 37°C by approximately 18°. Below the LCST, the PNIPAAm grafted surface is relatively hydrophilic presumably due to hydrogen bonding between the amide group of polymer chains and water [54] which results in a relatively low contact angle when compared to contact angle measured at temperatures well above its LCST. Above the LCST (>32°), due to the breaking of the hydrogen bonding results in collapsed polymer chains and the surface behaves relatively hydrophobic [59].

It should be noted that eq. (4) used for calculating surface shear force is valid for only laminar flow conditions and provided that the radius of the disk (R) is large compared to the boundary layer of fluid (δ) carried with the disk given by eq. (5).

$$\delta = 3.6 \left(\frac{\mu}{\rho\omega}\right)^{1/2} \qquad \text{eq. (5)}$$

The custom-built spinning disk has dimensions (scheme 2) that ensure characterized laminar flow patterns within the range of rotational speed (0 – 4000 rpm) in

which we performed our experiments. For instance, for an angular speed of 4000 rpm (the maximum rpm used in our experiments) operated at 22°C, the resulting δ is 0.057 mm. Thus for the spinning disk apparatus (R = 12.5mm), the infinite disk approximation is valid ($R/\delta > 50$). For this speed, the characteristic Reynolds number ($Re = \rho\omega R^2/\mu$) is 9 x 10^4, resulting in a laminar flow field ($Re_{crit} = 3.0 \times 10^5$) [123].

In Fig. 3.2a, the curve represents data points obtained from five similar identical samples and each data point is an average of six values taken across a known radial circumference. The standard deviation errors lie within the size of the data points which ensures the uniform shear force gradient acting across the sample surface. An insight into Fig. 3.2a and 3.2b together clearly indicate that though the amount shear force acting at a particular radial position r changes with the rotation speed, ω of the spinning disk, they remain consistently correlated and does not show any variation from one sample to another (i.e., the fraction of adherent cells strictly depends on the shear rate irrespective of variations within r and ω for a constant shear force).

Our group have previously reported that *C. marina* adheres more readily to hydrophobic surfaces relative to hydrophilic surfaces [47, 52]. Okano *et al.* have postulated for eukaryotic cells that above the LCST, the physic-chemical properties of the collapsed surface enable cell adhesion, and when the temperature is lowered below LCST hydration of polymer surface causes a decrease in the adhesion strength of the cell to the surface [138, 139] . In Fig. 3.3 it is clear that detachment at 37°C (> LCST) is different from detachment at 4°C and 22°C (< LCST) indicating that the detachment mechanism is relatively more dependent on thermo-responsive behavior of PNIPAAm than on shear

force applied. However, the reasons for the detachment curve at 37°C showing a constant profile are still not clearly known, and we are currently investigating the reasons for this observation. We hypothesize that bacterial cells may be attaching to these surfaces with a different kind of orientation or surface area depending on the surface behavior of PNIPAAm above and below its LCST. Dalton et al. [140] found that for a marine pseudomonad, the morphology of entire colonies formed on hydrophobic surfaces differed greatly from the morphology of colonies formed on hydrophilic surfaces. Our first attempt of scanning electron microscope (SEM) studies did not yield any conclusive results about attachment pattern of cells to surfaces, but residue spots of detached cells and extracellular polymeric substances (EPS) of cells shearing-off from the substrate for cells which still remain adhered were observed (figure not shown). Also, the surface of the cells as examined through SEM observed to be relatively rough compared to our previous results where cells are not subjected to shear indicating a change in the surface morphology of cells in the presence of an external shear force. However, we intend to repeat and continue our SEM studies and also verify how loss of resilience of the polymer upon repetitive use which we observed earlier would affect the detachment experiments under shear [52].

From Fig. 3.4a and 3.4b it is evident that time period of attachment significantly affects the efficiency for release of attached cells from PNIPAAm brushes. Our previous studies on *C. marina* attachment to plasma cleaned polystyrene, PNPAAm, and glass surfaces showed larger population of cell densities on surfaces upon longer incubation times and also amount of cell release under low-shear (ordinary rinsing) had significant

differences depending on incubation time periods [53]. Here (Fig. 3.4a and 3.4b), we notice a drastic decrease in the fractional cell release of more than 50% for thin polymer brushes (19 nm) in comparison to thick brushes (90 nm).

Investigations into the influence of the properties of electron beam-grafted PNIPAAm layers on cellular behavior revealed that the layer thickness play a critical role in cell adhesion and detachment [141]. Kikuchi and Okano suggested that this dependence of cell behavior on the thickness of PNIPAAm layer is due to an enhanced or limited mobility of the grafted polymer chains, which in turn depended on the grafting density, hydration and temperature [142]. Another possible reason might be the role of polymer surface roughness on the cell adhesion strength, based on the fact that the GPC results (chapter 2) showed higher PDI for larger molecular weight polymers. Also, Jacobs *et al.* have previously proved that polymeric materials demonstrated significant increased adhesion strength associated with increased surface roughness [143]. We intend to investigate in future studies, the cell attachment/release to PNIPAAm brushes of intermediate thickness (40-50 nm) followed by SEM studies to investigate if we can observe a direct correlation between the polymer brush thickness and surface roughness to cell detachment under shear. Cremer *et al.* asserted that Hoffmeister salts alter the LCST of PNIPAAm influenced by the interaction between the anions of salt (dissolved in water), PNIPAAm and its hydration waters [144]; they even investigated and proposed that the extent this “salting in/out” effect on LCST depends on the molecular weight of PNIPAAm [145]. Hence, we also propose to study the effect of Hoffmeister salts present

in artificial and natural sea water on the LCST and attachment/detachment of cells from PNIPAAm grafted surfaces.

Chapter 4

Conclusions and Recommendations for Future Work

4.1 Conclusions

4.1.1 New Method of Synthesis and Characterization of PNIPAAm Grafted Surfaces Using ARGET ATRP in Presence of Air for Cell Adhesion Studies.

ARGET (activators regenerated by electron transfer) ATRP enables the successful synthesis of well defined PNIPAAm polymer even in the absence of inert environments (e.g. Schlenk line or glove box), using very low concentrations of copper catalyst (~ 100 ppm). The process utilizes copper(II) complex which is continuously reduced to copper(I) complex in the presence of ascorbic acid or tin(II) 2-ethylhexanoate. However, surface grafting of PNIPAAm polymer using tin(II) 2-ethylhexanoate retained traces of tin which may be toxic to marine micro-organisms and other biological organisms. The use of ascorbic acid allowed the controlled polymerization of PNIPAAm as analyzed by various characterization techniques such as XPS, ToF-SIMS, FTIR and GPC and therefore has a profound implication for fast and easy large-scale synthesis of PNIPAAm homopolymer and various copolymers.

4.1.2 Thermo-Responsive Polymers for Quantitative Cell Adhesion Studies Using Spinning Disk Apparatus

Spinning disk apparatus provide a precise method for measuring cell adhesion strength to the proposed anti-biofouling surfaces using reproducible known shear forces caused by the fluid flow. PNIPAAm grafted surfaces showed a non-linear cell detachment profile of adhered *C. marina* bacteria with respect to known shear rate and resulted in a substantial 50% additional release at temperature below the LCST relative to temperature above the LCST exemplifying the affinity of *C. marina* to hydrophobic surfaces and the use of thermally responsive polymeric materials to reversibly attach/detach marine micro-organisms to control biofouling. The experiments conducted also conspicuously illustrate that PNIPAAm brush thickness and time period of cell adherence plays a prominent role in cell release and cell adhesion strength both above and below the LCST of PNIPAAm. There could be many possible reasons for this contradistinguished effect which needs further investigation and study both theoretically and experimentally.

4.2 Recommendations for Future Work

Further study of reaction kinetics of PNIPAAm polymerization reaction using reducing agent is recommended such as carrying out the polymerization reaction with various concentration of reducing agent, metal/ligand complex, monomer concentration as done by other researchers for different ATRP techniques [91, 146, 147]. This can help use in understanding the exact possible reasons for non-linear brush growth at

polymerization time above 9 minutes. In order to verify the proposed assumption of increases in surface roughness at higher polymerization time based on higher poly dispersities (PDI), AFM studies are recommended both in air and water media which can also provide us detailed information regarding surface roughness and also surface defects.

We are ardent for doing SEM analysis of samples following spinning disk experiments to understand the surface adhesion and its effect on bacteria under shear both above and below the LCST of PNIPAAm. Using spinning disk apparatus, we also intend to analyze the cell adhesion strength to grafted PNIPAAm surfaces for bacteria which we have proved earlier to have relative adhesion preferences to hydrophilic surfaces (e.g. *Staphylococcus epidermidis*) [49, 52] and verify if the same detachment profiles are observed, but under opposite transition temperatures. We are even interested in performing spinning disk experiments for a series of SAM immobilizes surfaces (e.g. OEG series) which we are presently investigating in our lab for their surface energies and bacterial adhesions followed by cell adhesion/release studies on patterned SAM and PNIPAAm surfaces produced using interferometric lithography [148-150].

References

1. Costerton J. W., Cheng K. J., Gessey G. G., Ladd T. I., Nickel J. C., Dasgupta M., Marrie T. J., Bacterial biofilms in nature and disease. *Ann Rev Microbiol*, 1987, **41**, p: 435-464.
2. Stoodley P., Sauer K., Davies D. G., Costerton J.W., Biofilms as complex differentiated communities. *Ann. Rev. Microbiol.*, 2002, **56**, p: 187-209.
3. Callow J. A., Callow M. E., Biofilms. *Prog. Mol. Subcell Biol* 2006, **42**, p: 141-169.
4. Stoodley L. H., Stoodley P., Evolving concepts in biofilm infections. *Cellular Microbiology*, 2009, **7**, p: 1034-1043.
5. Flemming H-C, Murthy P. S., Venkatesan R., Cooksey K., Marine and Industrial Biofouling. *Springer Series on Biofilms*, 2009, **4**.
6. Callow M. E., Callow J. A., Clare A. S., Some new insights into marine biofouling. *Paints & Coatings, World Super Yatch*.
7. Stoodley L. H., Costerton J. W., Stoodley P., Bacterial biofilms: From the natural environment to infectious diseases. *Nature Reviews*, 2004, **2**, p: 95-108.
8. Bott T. R., Biofilms in process and industrial waters: the biofilm ecology of microbial biofouling, biocide resistance and corrosion. *In : Keevil CW, Godfree A,*

References

Holt D, Dow C (eds.) Biofilms in the aquatic environment, Royal Society of Chemistyr, London, 1999, p: 80-92.

9. Bott T. R., The control of biofilms in industrial cooling water systems. *In: Wimpenny W, Nichols D, Sticker, Lappin-Scott H (eds.) Bacterial biofilms and their control in medicine and industry Bioline, Cardiff*, 1994.
10. Characklis W. G, Marshall K., Biofilms: a basis for an interdisciplinary approach. *Wiley New York*, 1990, p: 3-15.
11. Bott T. R., Fouling of heat exchangers. *Elsevier, Amsterdam*, 1995, p: 524.
12. Camper, A. K., Coliform regrowth and biofilm accumulation in drinking water systems: a review. *In: Geesey CG, Lewandowski Z, Flemming HC (eds.) Biofouling/biocorrosion in industrial systems Lewis Chelsea, MI*, 1993.
13. Gotz, F., Staphylococcus and biofilms. *Mol. Microbiol*, 2002, **43**, p: 1367–1378.
14. von Eiff C., Heilmann C., Hermann M., Peters G., Basic aspects of the pathogenesis of staphylococcal polymerassociated infections. *Infection,* 1999, **27**, p: S7–S10.
15. Bryers J. D., Medical Biofilms. *Biotechnol Bioeng*, 2008, **100**, p: 1-18.
16. Busscher H. J., Bos J. C., van der Mei H., , Initial microbial adhesion is a determinant for the strenght of biofilm adhesion. *FEMS Microbiol. Lett.*, 1995, **128**(229-234).
17. Callow J. A., Callow M. E., Ista L. K., Lopez G. P., Chaudhury M. K., The influence of surface energy on the wetting behaviour of the spore adhesive of the

marine alga Ulva linza (synonym Enteromorpha linza). *J. R. Soc. Interface*, 2005, **2**, p: 319-325.

18. Beer D. D., Stoodley P., Microbial Biofilms. *Prokaryotes*, 2006, **1**, p: 904-937.
19. Kiil S., Dam-Johansen K., Weinell C. E., Pedersen M. S., Codolar S .A., Dynamic simulations of a self-polishing antifouling paint exposed to seawater. *Journal of Coatings Technology*, 2002, **74**, p: 89-91.
20. White D. C., Kirkegaard R. D., Palmer Jr. R. J., Flemming C. A., Chen G., Leung K. T., Phiefer C. B., Arrage A. A., The biofilm ecology of microbial biofouling, biocide resistance and corrosion. *Biofilms in the Aquatic Environment*, 1997, p: 120~130.
21. Callow M. E., Callow J. A., Marine biofouling: a sticky problem. *Biologist*, 2002, **49**, p: 1-5.
22. Schultz, M. P., Effect of coating roughness and biofouling on ship resistance and powering. *Biofouling*, 2007, **23**, p: 331-341.
23. Ingle, M., presented at the ONR Program Review, Charleston, SC (unpublished). 2008.
24. Roberts, L., Zebra mussel invasion threatens United States waters. *Science*, 1999, **249**, p: 1370-1372.
25. Chambers L. D., Stokes K. R., Walsh F. C., Wood R. J. K.,, Modern approaches to marine antifouling coatings. 2006, **201**, p: 3642–3652.

References

26. Abbott A., Abel P.D., Arnold D.W., Milne A., Cost-benefit analysis of the use of TBT: The case for a treatment approach. *The Science of the Total Environment*, 2000, **258**, p: 5-19.

27. Characklis, W. G., Microbial biofouling, In. *Biofouling*, 1990, **Marshall, K. C., Ed. Wiley: New York**.

28. Vladkova, T., Surface Modification Approach to Control Biofouling. *Marine and Industrial Biofouling, Springer Series on Biofilms*, 2008, **4**, p: 135-163.

29. Kiil Y. S., Dam-Johansen K., Antifouling technology—past, present and future steps towards efficient and environmentally friendly antifouling coatings. *Prog Org Coat*, 2004, **50**, p: 75-104.

30. Howell D., Behrends B., A review of surface roughness in antifouling coatings illustrating the importance of cutoff length. *Biofouling*, 2006, **22**, p: 401-410.

31. Ozretic B., Petrovic S., Ozretic M. K., Toxicity of TBT-based paint leachates on the embryonic development of the sea urchin Paracentrotus lividus Lam. *Chemosphere*, 1998, **37**, p: 1109-1118.

32. Evans S. M., Leksono T., McKinnell P. D., Tributyltin Pollution: A Diminishing Problem Following Legislation Limiting the Use of TBT-Based Anti-fouling Paints. *Mar. Pollut. Bull.*, 1995, **30**, p: 14-21.

33. Swain, G., Proceedings of the International Symposium on Sea water Drag Reduction, The Naval Undersea Warfare Center, Newport,. 1998, p: 155-161.

References

34. Champ, M. A., A review of organotin regulatory strategies, pending actions, related costs and benefits. *The Science of the Total Environment*, 2000, **258**, p: 21-71.

35. Turner A., Singha N., Richardsa P., Bioaccessibility of metals in soils and dusts contaminated by marine antifouling paint particles. *Environ. Pollut.*, 2009, **15**, p: 1526–1532.

36. Mudryk, Z. J., Antibiotic resistance among bacteria inhabiting surface and subsurface water layers in estuarine lake Gardno. *Pol. J. Environ. Stud.*, 2002, **11**, p: 401-406.

37. Kobori H., Sullivan C.W., Shizuya H., Bacterial plasmids in Antarctic natural microbial assemblages. *J. Appl. Environ. Microbiol.*, 1984, **48**, p: 515-518.

38. Terlezzi A., Conte E., Zupo V., Mazzella L., Biological succession on silicone fouling-release surfaces: long term exposure tests in the harbour of Ischia, Italy. *Biofouling*, 2000, **15**, p: 327-342.

39. Steinberg P. D., de Nys R., Kjelleberg S., Chemical defenses of seaweeds against microbial colonization. *Biodegration*, 1997, **8**, p: 211-220.

40. Armstrong E., Boyd K. G., Pisacane A., Peppiatt C. J., Burgess J. G., Marine microbial natural porducts in antifouling coatings. *Biofouling*, 2000, **16**, p: 215-224.

41. Tirrschof, D., Natural product anifoulants: one perspective on the challenges related to coatings development. *Biofouling*, 2000, **15**, p: 119-127.

References

42. Baier, R. E., Surface behaviour of biomaterials: The theta surface for biocompatibility. *J Mater Sci: Mater Med*, 2006, **17**, p: 1057-1062.

43. Roberts C., Chen C. S., Mrksich M., Martichonok V., Ingber D. E., Whitesides G. M., Using Mixed Self-Assembled Monolayers Presenting RGD and (EG)3OH Groups To Characterize Long-Term Attachment of Bovine Capillary Endothelial Cells to Surfaces. *J. Am. Chem. Soc.*, 1998, **120**, p: 6548-6555.

44. Herrwerth S., Eck W., Reinhardt S., Grunze M., Factors that Determine the Protein Resistance of Oligoether Self-Assembled Monolayers − Internal Hydrophilicity, Terminal Hydrophilicity, and Lateral Packing Density. . *Am. Chem. Soc.*, 2003, **125**, p: 9359–9366.

45. Balamurugan S., Ista L. K., Yan J., López G. P., Fick J., Himmelhaus M., Grunze M., Reversible Protein Adsorption and Bioadhesion on Monolayers Terminated with Mixtures of Oligo(ethylene glycol) and Methyl Groups. *J. Am. Chem. Soc.*, 2005, **127**, p: 14548–14549.

46. Callow M. E., Callow J. A., Ista L. K., Coleman S. E., Nolasco A. C., Lopez G. P., Use of Self-Assembled Monolayers of Different Wettabilities To Study Surface Selection and Primary Adhesion Processes of Green Algal (Enteromorpha) Zoospores. *Appl. Environ. Microbiol.*, 2000, **66**, p: 3249-3254.

47. Ista L. K., Fan H., Baca O., Lopez G. P., Attachment of bacteria to solid model surfaces: oligo(ethylene glycol) surfaces inhibit bacterial attachment. *FEMS Microbiol. Lett.*, 2006, **142**, p: 59-63.

References

48. Reed J., Lucero A. E., Hu S., Ista L. K., Bore M. T., Lo´pez G. P., Canavan H. E., A Low-Cost, Rapid Deposition Method for "Smart" Films: Applications in Mammalian Cell Release. *ACS Appl. Mater. Interfaces*, 2010, **2**, p: 1048-1051.

49. Ista L. K., Mendez S., Lopez G. P., Attachment and detachment of bacteria on surfaces with tunable and switchable wettability. *Biofouling*, 2010, **26**, p: 111-118.

50. Callow M. E., Fletcher R. L., The Influence of Low Surface Energy Materials on Bioadhesion - a Review. *International Biodeterioration & Biodegradation*, 1994, p: 333-348.

51. Ista L. K., Mendez S., Perez-Luna V. H., Lopez G. P., Synthesis of Poly(N-isopropylacrylamide) on Initiator-Modified Self-Assembled Monolayers. *Langmuir*, 2001, **17**, p: 2552-2555.

52. Ista L. K., Perez-Luna V. H., Lopez G. P., Surface-Grafted, Environmentally Sensitive Polymers for Biofilm Release. *Appl. Environ. Microbiol.*, 1999, **65**, p: 1603-1609.

53. Ista L. K., Lopez G. P., Lower critical solubility temperature materials as biofouling release agents. *Journal of Industrial Microbiology & Biotechnology*, 1998, **20**, p: 121-125.

54. Alarcon C. H., Pennadam S., Alexander C., Stimuli responsive polymers for biomedical applications. *Chemical Society Reviews*, 2004, **34**, p: 276–285.

References

55. Reed J. A., Love S., Lucero A. E., Haynes C., Canavan H. E., Effect of polymer deposition method on thermoresponsive polymer films and resulting cellular behavior. 2010, Submitted to Langmuir.

56. Yamato M., Konno C., Utsumi M., Kikuchi A., Okano T.,, Thermally responsive polymer-grafted surfaces facilitate patterned cell seeding and co-culture. *Biomaterials*, 2002, **23**, p: 561-567.

57. Cunliffe D., Alarcon C. H., Peters V., Smith J.R., Alexander C., Thermoresponsive Surface-Grafted Poly(N−isopropylacrylamide) Copolymers: Effect of Phase Transitions on Protein and Bacterial Attachment. *Langmuir*, 2003, **19**, p: 2888-2899.

58. Lebon F., Caggioni M., Bignotti F., Abbate S., Gangemi F., Longhi G., Mantegazza F., Bellini T., Coil-to-Globule Transition of Poly(N-isopropylacrylamide) Doped with Chiral Amino Acidic Comonomers. *J. Phys. Chem. B*, 2007, **111**, p: 2372–2376.

59. Chen M., Dong M., Havelund R., Regina V. R., Meyer R. L., Besenbacher F., Kingshott P., Thermo-Responsive Core-Sheath Electrospun Nanofibres from Poly (*N*-isopropylacrylamide)/Polycaprolactone Blends. *Chem. Mater.*, 2010, **22**, p: 4214-4221.

60. Luzinov I., Minko S., Tsukruk V., Responsive brush layers: from tailored gradients to reversibly assembled nanoparticles. *Soft Matter*, 2008, **4**, p: 714– 725.

References

61. Luzinov I., Minko S., Tsukruk V. V., Adaptive and responsive surfaces through controlled reorganization of interfacial polymer layers *Prog. Polym. Sci.*, 2004, **29**, p: 635– 698.

62. Minko, S., Responsive Polymer Brushes *Polym. Rev.*, 2006, **46**, p: 397– 420.

63. Hoffman, A. S., Environmentally Sensitive Polymers and Hydrogels. *MRS Bull.*, 1991, p: 42-46.

64. Galaev, Yu., 'Smart' polymers in biotechnology and medicine. *Russ. Chem. Rev.*, 1995, **64**, p: 471–489.

65. Schild, H. G., Poly(N-isopropylacrylamide): experiment, theory and application. *Prog. Polym. Sci.*, 1992, **17**, p: 163-249.

66. Hoffman, A. S., Applications of thermally reversible polymers and hydrogels in therapeutics and diagnostics. *J. Control. Rel.*, 1987, **6**, p: 297-305.

67. Bae Y. H., Okano T., Kim S. W., Temperature dependence of swelling of crosslinked poly(N,N′-alkyl substituted acrylamides) in water. *J Poly. Sic.*, 1990, **28**, p: 923-936.

68. Kidchob T., Kimura S., Imanishi Y., Degradation and release profile of microcapsules made of poly[Image -lactic acid-co-Image -lysine(Z)] *J. Contr. Rel.*, 1998, **54**, p: 283-292

69. Rao G. V. R., Krug M. E., Balamurugan S., Xu H. F., Xu Q., Lopez, G. P., Synthesis and Characterization of Silica−Poly(N-isopropylacrylamide) Hybrid Membranes: Switchable Molecular Filters. *Chem. Mater.*, 2002, **14**, p: 5075–5080.

References

70. Kanazawa H., Sunamoto T., Ayano E., Matsushima Y., Kikuchi A., Okano T., Temperature-Responsive Chromatography Using Poly-(N-isopropylacrylamide) Hydrogel-Modified Silica. *Anal Sci*, 2002, **18**, p: 45-48.

71. Okano T., Kikuchi A., Sakurai Y., Takei Y., Ogata N.,, Temperature-responsive poly(N-isopropylacrylamide) as a modulator for alteration of hydrophilic/hydrophobic surface properties to control activation/inactivation of platelets. *J. Contr. Rel.*, 1995, **36**, p: 125-133.

72. Huber D. L., Maginell R. P., Samara M. A., Kim B.I., Bunker B. C., Programmed Adsorption and Release of Proteins in a Microfluidic Device. *Science*, 2003, **301**, p: 352-354.

73. Fu Q., Rao G. V. R., Basame S. B., Keller D. J., Artyushkova K., Fulghum J. E., López G. P., Reversible Control of Free Energy and Topography of Nanostructured Surfaces. *J. Am. Chem. Soc.*, 2004, **126**, p: 8904–8905.

74. Tu H., Heitzman C. E., Braun P. V., Patterned poly(N-isopropylacrylamide) brushes on silica surfaces by microcontact printing followed by surface-initiated polymerization

Langmuir, 2004, **20**, p: 8313-8320.

75. Zhao B., Brittain W. J., Polymer Brushes: Surface-Immobilized Macromolecules. *Prog. Polym. Sci.*, 2000, **25**, p: 677-710.

76. Prucker O., Ruhe J., Synthesis of Poly(styrene) Monolayers Attached to High Surface Area Silica Gels through Self-Assembled Monolayers of Azo Initiators. *Macromolecules*, 1998, **31**, p: 592-601.

References

77. Matyjaszewski, K., Controlled/Living Radical Polymerization: Progress in ATRP. *American Chemical Society*, 2009, **1023**, p: 3-13.

78. Curran, D. P., *Comprehensive Organic Synthesis*, 1992, **New York**.

79. Wang J.S., Matyjaszewski K., Controlled/"living" radical polymerization. atom transfer radical polymerization in the presence of transition-metal complexes. *J Am Chem Soc*, 1995, **117**, p: 5614-5615.

80. Kato M., Kamigaito M., Sawamoto M., Higashimura T., Polymerization of Methyl Methacrylate with the Carbon Tetrachloride/Dichlorotris-(triphenylphosphine)ruthenium(II)/Methylaluminum Bis(2,6-di-tert-butylphenoxide) Initiating System: Possibility of Living Radical Polymerization. *Macromolecules*, 1995, **28**, p: 1721-1723.

81. Matyjaszewski K., Xia J.H., Atom Transfer Radical Polymerization. *J. Chem. Rev.*, 2001, **101**, p: 2921−2990.

82. Gao H., Tsarevsky N. V., Matyjaszewski K., Synthesis of Degradable Miktoarm Star Copolymers via Atom Transfer Radical Polymerization. *Macromolecules* 2005, **38**, p: 5995−6004.

83. Davis K. A., Matyjaszewski K., Statistical, Gradient, Block, and Graft Copolymers by Controlled/Living Radical Polymerizations *Adv. Polym. Sci.*, 2002, **159**, p: 1−166.

84. Coessens V., Pintauer T., Matyjaszewski K., Functional polymers by atom transfer radical polymerization *Prog. Polym. Sci.* , 2001, **26**, p: 337−377.

References

85. Edmondson S., Osborne V. L., Huck W. T., Polymer brushes via surface-initiated polymerizations. *Chem. Soc. Rev.*, 2004, **33**, p: 14−22.

86. Azzaroni O., Brown A. A., Huck W. T. S., UCST wetting transitions of polyzwitterionic brushes driven by self-association. *Chem., Int. Ed.*, 2006, **45**.

87. Licciardi M., Tang Y., Billingham N. C., Armes S. P., Lewis A. L., Synthesis of Novel Folic Acid-Functionalized Biocompatible Block Copolymers by Atom Transfer Radical Polymerization for Gene Delivery and Encapsulation of Hydrophobic Drugs. *Biomacromolecules*, 2005, **6**, p: 1085−1096.

88. Chen G., Huynh D., Felgner P. L., Guan Z. J., Tandem Chain Walking Polymerization and Atom Transfer Radical Polymerization for Efficient Synthesis of Dendritic Nanoparticles for Bioconjugation. *J. Am. Chem. Soc.*, 2006, **128**, p: 4298−4302.

89. Plunkett K. N., Zhu X., Moore J. S., Leckband D. E., PNIPAM Chain Collapse Depends on the Molecular Weight and Grafting Density. *Langmuir*, 2006, **22**, p: 4259-4266.

90. Costerton, J. W., Bacterial biofilms in nature and disease. *Ann. Rev. Microbiol.*, 1987, **41**, p: 435-464.

91. Matyjaszewski K., Dong H., Jakubowski W., Pietrasik J., Kusumo A., Grafting from Surfaces for "Everyone": ARGET ATRP in the Presence of Air. *Langmuir*, 2007, **23**, p: 4528-4531.

References

92. Tomislav P., Matyjaszewski K., Atom transfer radical addition and polymerization reactions catalyzed by ppm amounts of copper complexes. *Chemical Society Reviews*, 2008, **37**(6), p: 1087.

93. Matyjaszewski K., Patten T. E., Xia J. H., Controlled/Living Radical Polymerization - Kinetics of the Homogeneous Atom-Transfer Radical Polymerization of Styrene. *Journal of the American Chemical Society*, 1997, **119**(4), p: 674-680.

94. Fischer, H., The persistent radical effect in controlled radical polymerizations. *Journal of Polymer Science Part A: Polymer Chemistry*, 1999, **37**, p: 1885–1901.

95. Kajiwara A., Matyjaszewski K., Kamachi M., Simultaneous EPR and Kinetic Study of Styrene Atom Transfer Radical Polymerization (ATRP). *Macromolecules*, 1998, **31**, p: 5695-5701.

96. Gotoa A., Fukuda T., Kinetics of living radical polymerization *Progress in Polymer Science*, 2004, **29**, p: 329-385.

97. Tang W., Tsarevsky N. V., Matyjaszewski K., Determination of Equilibrium Constants for Atom Transfer Radical Polymerization. *J. Am. Chem. Soc.*, 2005, **128**, p: 1598-1604.

98. Braunecker W. A., Tsarevsky N. V., Pintauer T., Gil R. R., Matyjaszewski K., Quantifying Vinyl Monomer Coordination to CuI in Solution and the Effect of Coordination on Monomer Reactivity in Radical Copolymerization. *Macromolecules*, 2005, **38**(10), p: 4081-8.

References

99. Braunecker W. A., Pintauer T., Tsarevsky N. V., Kickelbick G., Matyjaszewski K., Towards Understanding Monomer Coordination in Atom Transfer Radical Polymerization: Synthesis of [CuI(PMDETA)(π-M)][BPh_4] (M = Methyl Acrylate, Styrene, 1-Octene, and Methyl Methacrylate) and Structural Studies by FT-IR and ^{1}H NMR Spectroscopy and X-ray Crystallography. *J. Organometal. Chem.*, 2005, **690**, p: 916-924.

100. Banu N., Tsuchiya T., Sawada R., Effects of Tin Compounds on Human Chondrogenic Activity In Vitro. *Animal Cell Technology: Basic & Applied Aspects*, 2009, **15**, p: 181-186.

101. Banu N., Tsuchiya T., Sawada R., Effects of a biodegradable polymer synthesized with inorganic tin on the chondrogenesis of human articular chondrocytes. *Journal of Biomedical Materials Research Part A*, 2006, **77A**, p: 84–89.

102. Jackson, J. E., Principal compoment and factor analysis. *J. Qual. Technol.*, 1980, **12**, p: 201-213.

103. Wold S., Esbensen K., Geladi P., Principal component analysis. *Chemom. Intell. Lab. Syst.* , 1987, **2**, p: 37-52.

104. Gordon A. J., Ford R. A., The Chemist's Companion: A Handbook of Practical Data, Techniques, and References. *John Wiley & Sons*, 1972.

105. Lutz J. F., Matyjaszewski k., Kinetic Modeling of the Chain-End Functionality in Atom Transfer Radical Polymerization. *Macromol. Chem. Phys.*, 2002, **203**, p: 1385-1395.

References

106. Drelick J., Miller J. D., A systematic comparison of sessile-drop and captive-bubble contact angle methods. *SME Annual Meeting, Denver, Colorado, March 6-9*, 1995.

107. Fitzpatrick S. D., Mazumder M. A. J., Lasowski F., Fitzpatrick L. E., Sheardown H., PNIPAAm-Grafted-Collagen as an Injectable, In Situ Gelling, Bioactive Cell Delivery Scaffold. *Biomacromolecules*, 2010, **11**, p: 2261–2267.

108. Ista L. K., Callow M. E., Finlay J. A., Coleman S. E., Nolasco A. C., Callow J. A., Lopez G. P., Effect of substratum surface chemistry and surface energy on attachment of marine bacteria and algal spores. *Appl Environ Microbiol*, 2004, **70**, p: 4151-4157.

109. Ista L. K., Fan H., Baca O., Lopez G. P., Attachment of bacteria to model solid surfaces: oligo(ethylene glycol) surfaces inhibit bacterial attachment. *FEMS Microbiol. Lett.*, 1996, **142**, p: 59-63.

110. Jucker B. A., Zehnder A. J. B. Harms H., Quantification of polymer interaction in bacterial adhesion. *Environ. Sci. Tech-nol.*, 1998, **32**, p: 2909-2915.

111. Fletcher, M., Bacterial attachment in aquatic environments: a diversity of surfaces and adhesion strategies. In: Fletcher, M. (Ed.), Bacterial Adhesion: Molecular and Ecological Diversity. *Wiley–Liss, New York*, 1996.

112. Razatos A., Ong Y. -L., Sharma M. M., Georgiou G., Molecular determinants of bacterial adhesion monitored by atomic force microscopy. *Proc. Natl. Acad. Sci. USA.*, 1998, **95**, p: 11059-11064.

References

113. Gannon J. T., Manilal, V. B., Alexander M., Relationship between cell surface properties and transport of bacteria through soil. *Appl. Environ. Microbiol.*, 1991, **57**, p: 190-193.

114. Busscher H. J., Weerkamp A. H., van der Mei H. C., van Pelt A. W. J., De Jong H. P., Arends J., Measurements of the surface free energy of bacterial cell surfaces and its relevance for adhesion. *Appl. Environ. Microbiol.*, 1984, **48**, p: 980-983.

115. McKeever, P.E., Methods to study pulmonary alveolar macrophage adhesion: micromanipulation and quantification. *J Reticuloendothelial Soc*, 1974, **16**, p: 313-317.

116. Cao T., Tang H. Y., Liang X. M., Wang A. F., Auner G. W., Salley S. O., Ng K. Y. S., Nanoscale investigation on adhesion of E. coli surface modified silicone using atomic force microscopy. *Biotechnol Bioeng*, 2006, **94**, p: 167-176.

117. Fallman E., Schedin S., Jass J., Andersson M., Uhlin B. E., Axner O., Optical tweezers based force measurement system for quantitating binding interactions: system design and application for the study of bacterial adhesion. *Biosens Bioelectron*, 2004, **19**, p: 1429-1437.

118. Walker S. L., Redman J. A., Elimelech M., Role of cell surface lipopolysaccharides in Escherichia coli K12 adhesion and transport. *Langmuir*, 2004, **20**, p: 7736–7746.

References

119. Meinders J. M., Van der Mei H. C., Busscher H. J., Deposition efficiency and reversibility of bacterial adhesion under flow. *J Colloid Interface Sci*, 1995, **176**, p: 329–341.

120. Bakker D. P., Busscher H. J., Van der Mei H. C., Bacterial deposition in a parallel plate and a stagnation point flow chamber: microbial adhesion mechanisms depend on the mass transport conditions. *Microbiology*, 2002, **148**, p: 597-603.

121. Horbett T. A., Waldburger J. J., Ratner B. D., Hoffman A. S., Cell adhesion to a series of hydrophilic-hydrophobic copolymers studied with a spinning disc apparatus. *J. Biomed. Mater. Res*, 1988, **22**, p: 383-404.

122. Fryer P. J., Slater N. K. H., Duddridge J. E., Suggestions for the Operation of Radial Flow Cells in Cell Adhesion and Biofouling Studies. *Biotechnology and Bioengineering*, 1985, **27**, p: 434–438.

123. Garcia A. J., Ducheyne P., Boettiger D., Quantification of cell adhesion using a spinning disc device and application to surface-reactive materials. *Biomaterials*, 1997, **18**, p: 1091-1098.

124. Nathan D. G., Garcia A. J., Quantitative Analyses of Cell Adhesion Strenght. *Methods in Molecular Biology: Adhesion protein protocols, Second Edition*, 2007, **370**, p: 83-95.

125. Sparrow E. M., Gregg J. L., Mass transfer, flow, and heat transfer about a rotating disk *J. Heat Transfer, Trans. ASME*, 1960, p: 294-302.

126. Levich, V.G., Physicochemical Hydrodynamics. *Prentice Hall, Englewood Cliffs, NJ*, 1962.

References

127. Serad, G., Chemical hydrodynamics with a rotating disk. PhD thesis. *University of Pennsylvania, Philadelphia, PA*, 1964.

128. Schlichting, H., Boundary-layer theroy. *6th Ed., Mc-Graw-Hill, NY*, 1968.

129. Kersters, K., The genus *Deleya* In: Balows A, Truper HG, Dworkin, Harder W, Schliefer KH, editors. *The Prokaryotes, a handbook on the biology of bacteria, ecophysiology, isolation, identification, application*, 1992, **2nd ed., New York: Springer Velag**, p: 3189-3197.

130. Baumann L., Baumann P., Mandel M., Allen R. D., Taxonomy of aerobic marine eubacteria. *J. Bacteriol*, 1972, **110**, p: 402-429.

131. Baumann L., Bowditch R. D., Baumann P., Description of *Deleya* gen. nov. created to accomodate the marine species of *Alcaligenes aestus*, *A. pacificus*, *A. cupidis*, *A. venustus*, and *Pseudomonas marina*. *Int J Syst Bacteriol*, 1983, **33**, p: 793-802.

132. Arahal D. L., Castillo A. M., Ludwig W., Schliefer K. H., Ventosa A., Proposal of Cobetia marina gen. nov, comb. nov., within the family Halomonadaceae, to include the species Halomonas marina. *Syst Appl Microbiol*, 2002, **25**, p: 207-211.

133. Frank J., Millero, Lepple F. K., The density and expansibility of artificial seawater solutions from 0 to 40°C and 0 to 21% chlorinity. *Marine Chemistry*, 1973, **1**, p: 89-104.

134. Fenton E. M., Mascarenas M. R., Lopez G. P., Sibbet S. S., Multiplex Lateral-Flow Test Strips Fabricated by Two-Dimensional Shaping. *Applied Interfaces and Materials*, 2009, **1**, p: 124–129.

References

135. Mendez S., Fenton E. M., Gellegos G. R., Petsev D. N., Sibbet S. S., Stone H. A., Zhang Y., Lopez G. P., Imbibition in Porous Membranes of Complex Shape: Quasi-stationary Flow in Thin Rectangular Segments. *Langmuir*, 2010, **26**, p: 1380–1385.

136. Burger, Burge Digital Image Processing: An algorithmic approach using Java. *Spring-Verlag, New York* 2008(ISBN 978-1-84628-379-6).

137. Burger, Burge, Principles of Digital Image Processing Fundamental Techniques. *Springer*, 2009(ISBN 978-1-84800-190-9).

138. Yomata M., Konno C., Kushida A., Hirose M., Mika V., Kikuchi A., Okano T., Release of adsorbed fibronectin from temperature-responsive culture surfaces requires cellular activity. *Biomaterials*, 2000, **21**, p: 981-986.

139. Okano T., Yamada N., Okuhara M., Sakai H., Sakura Y., Mechanism of cell detachment from temperature-modulated hydrophilic-hydrophobic polymer surfaces. *Biomaterials*, 1995, **16**, p: 297-303.

140. Dalton H. M., Poulsen L. K., Halasz P., Angles M. L., Goodman A. E., Marshall K. C., Substratum-induced morphological changes in a marine bacterium and their relevance to biofilms structure. *J. Bacteriol.*, 1994, **176**, p: 6900-6906.

141. Akiyama Y., Kikuchi A., Yamato M., Okano T., Ultrathin poly(N-isopropylacrylamide) grafted layer on polystyrene surfaces for cell adhesion/detachment control. *Langmuir*, 2004, **20**, p: 5506-5511.

References

142. Takahashi H., Nakayama M., Yamato M., Okano T., Controlled chain length and graft density of thermo responsive polymer brushes for optimizing cell sheet harvest. *Biomacromolecules,* 2010, **11**, p: 1991-1999.

143. Hallab N. J., Bundy K. J., O'Connor K., Moses R. L., Jacobs J. J., Evaluation of Mettalic and Polymeric Biomaterial Surface Energy and Surface Roughness Characteristics for Directed Cell Adhesion. *Tissue Engineering*, 2001, **7**, p: 55-71.

144. Zhang Y., Furyk S., Bergbreiter D. E., Cremer P. S., Specific ion effects on the water solubility of macromolecules: PNIPAAm and the Hofmeister series. *J. Am. Chem. Soc.*, 2005, **127**, p: 14505-14510.

145. Zhang Y., Furyk S., Sagle L.B., Cho Y., Bergbreiter D. E., Cremer P. S., Effect of Hofmeister anions on the LCST of PNIPAAm as a function of molecular weight. *J. Phys. Chem C.*, 2007, **111**, p: 8916-8924.

146. Pietrasik J., Dog H., Matyjaszewski K., Synthesis of High Molecular Weight Poly(styrene-co-acrylonitrile) Copolymers with Controlled Architecture. *Macromolecules*, 2006, **39**, p: 6348-6390.

147. Dong H., Matyjaszewski K., ARGET ATRP of 2-(Dimethylamino)ethyl Methacrylate as an Intrinsic Reducing Agent. *Macromolecules*, 2008, **41**, p: 6868-6870.

148. Johnson L. F., Kammlott G. W., Ingersoll K. A., Generation of Periodic Surface Corrugations. *Applied Optics,* 1978, **17**, p: 1165-1181.

149. Zaidi S. H., Brueck S. R. J., High Aspect-Ratio Holographic Photoresist Gratings. *Applied Optics,* 1988, **27**, p: 2999-3002.

References

150. Beesley M. J., Castledi.Jg, Use of Photoresist as a Halographic Recording Medium. *Applied Optics*, 1970, **9**, p: 2720-2724.